COORDINATION AND FREQUENCY CONTROL IN REDUCED MODELS OF LOCOMOTION PATTERN GENERATING CIRCUITS

by

Pamela Fiordilino

B.S., Montclair State University, 2014

Submitted to the Graduate Faculty of

the Kenneth P. Dietrich School of Arts and Sciences in partial

fulfillment

of the requirements for the degree of

Master of Science

University of Pittsburgh

2017

UNIVERSITY OF PITTSBURGH

KENNETH P. DIETRICH SCHOOL OF ARTS AND SCIENCES

This thesis was presented

by

Pamela Fiordilino

It was defended on

November 30, 2017

and approved by

Dr. Jonathan Rubin, Mathematics, University of Pittsburgh

Dr. Brent Doiron, Mathematics, University of Pittsburgh

Dr. David Swigon, Mathematics, University of Pittsburgh

Thesis Advisor: Dr. Jonathan Rubin, Mathematics, University of Pittsburgh

COORDINATION AND FREQUENCY CONTROL IN REDUCED MODELS OF LOCOMOTION PATTERN GENERATING CIRCUITS

Pamela Fiordilino, M.S.

University of Pittsburgh, 2017

The spinal hindlimb central pattern generators (CPGs) are capable of coordinating the hindlimbs in order to generate rhythmic activity in the absence of afferent feedback or rhythmic inputs. The flexibility and adaptability of CPGs allow them to initiate, modify and maintain phase relationships between excitatory and inhibitory neuron groups. Many half-center CPG models of intricate symmetric units have been studied. However, a complete understanding of oscillatory mechanisms that operate locomotion activity is yet to be achieved. This study explores a simplified computational model of excitatory and inhibitory CPG units within different regimes of escape and release mechanisms. Our study shows that one model of a CPG network can operate in many different regimes and produce pertinent locomotor-like activity and phase relationships. Numerical simulations and phase-plane analysis were used to compare responses in oscillation frequency and phase duration to the range of values of excitatory or inhibitory external drive or the strength of synaptic inhibition to one or two half-centers of the cells that initiate the dynamics. Our analysis shows that oscillatory frequency and phase duration changes are highly dependent on the different intrinsic characteristics of the driving cells and the mechanisms of escape and release that prescribe transitions between active and silent phases of each cell within the network. In particular, intrinsic escape regimes displayed large ranges in phase duration control while intrinsic release models displayed the greatest degree of independence in the asymmetric case. Also, in the symmetric case, excitatory cells exhibited a larger range of period activity with respect to the changes to the applied external drive throughout. These results are explained

using geometric phase plane analysis of the dynamics from explored regimes.

TABLE OF CONTENTS

PREFACE xii

1.0 INTRODUCTION 1

2.0 METHODS 9

2.1 CPG model 9

2.2 Computational model equations 11

2.3 Analysis of control of half-center oscillations and phase duration 16

3.0 ESCAPE MODEL 18

3.1 Excitatory Escape Model 19

3.1.1 Half-center oscillation mechanisms 19

3.1.1.1 Parameters 19

3.1.2 Control of oscillation period and phase duration 23

3.1.2.1 Symmetric case 23

3.1.2.2 Asymmetric case 25

3.2 Inhibitory Escape Model 27

3.2.1 Half-center oscillation mechanisms 27

3.2.1.1 Parameters 27

3.2.2 Control of oscillation period and phase duration 31

3.2.2.1 Symmetric case 31

3.2.2.2 Asymmetric case 32

4.0 RELEASE MODEL 35

4.1 Excitatory Release Model 35

4.1.1 Half-center oscillation mechanisms 35

4.1.1.1 Parameters . . . 36
4.1.2 Control of oscillation period and phase duration . . . 39
4.1.2.1 Symmetric case . . . 39
4.1.2.2 Asymmetric case . . . 41
4.2 Inhibitory Release Model . . . 43
4.2.1 Half-center oscillation mechanisms . . . 43
4.2.1.1 Parameters . . . 43
4.2.2 Control of oscillation period and phase duration . . . 46
4.2.2.1 Symmetric case . . . 46
4.2.2.2 Asymmetric case . . . 48
5.0 ADAPT ESCAPE AND RELEASE MODELS . . . 50
5.1 Adapt Inhibitory Escape Model . . . 51
5.1.1 Half-center oscillation mechanisms . . . 51
5.1.1.1 Parameters . . . 51
5.1.2 Control of oscillation period and phase duration. . . . 53
5.1.2.1 Symmetric case . . . 53
5.1.2.2 Asymmetric case . . . 55
5.2 Adapt Excitatory Release Model . . . 57
5.2.1 Half-center oscillation mechanisms . . . 57
5.2.1.1 Parameters . . . 57
5.2.2 Control of oscillation period and phase duration . . . 60
5.2.2.1 Symmetric case . . . 60
5.2.2.2 Asymmetric case . . . 61
6.0 CONCLUSIONS . . . 64
BIBLIOGRAPHY . . . 70

LIST OF TABLES

1 Constant Parameters 14
2 Parameters E-Escape 20
3 Parameters I-Escape 28
4 Parameters E-Release 36
5 Parameters I-Release 43
6 Parameters Adapt I-Escape 51
7 Parameters Adapt E-Release 57
8 Symmetric case 66
9 Asymmetric case 67
10 Asymmetric case 68

LIST OF FIGURES

1 **Organization of locomotor CPG's.** Schematic of interactions between the locomotor half-centers. The rhythm generator pairs consist of intrinsically excitatory cells (1 and 3) and intrinsically inhibitory cells (2 and 4). 11

2 Time courses for periodic oscillations of four cells (cell 1 (black), cell 2 (red), cell 3 (green), cell 4 (blue)) tuned to an excitatory escape regime. 21

3 Basic nullcline configurations and periodic orbits for a four cell network with half-center oscillation mechanism in an excitatory escape regime. The solid lines are v-nullclines. The red cubic curves represents the inhibited v-nullclines while the blue curves represent the uninhibited v-nullcline for cells 1 and 3. For cells 2 and 4 the red cubic curves represents its unexcited v-nullclines while the blue curves represent their excited v-nullcline. The dashed green lines are slow variable nullclines, thick black lines are trajectories corresponding to half-center oscillation, and "vertical" dotted lines show synaptic threshold. . . 22

4 Zoomed in image of cell 1 shows the range of possible solutions for $I_R = [h_{fP}(0), h_{RK}(s_{max})]$ that will ensure cells 1 and 3 are able to jump to the silent phase in segment I. 23

5 The periods of the basic periodic orbits shown in Figure 2 vary with changes in drive to both cells 1 and 3 24

6 **Nullcline variation changes of g_{appE} of excitatory cells:** The red nullclines represents the inhibited and uninhibited v-nullcline at its baseline g_{appE} drive. The purple nullclines shows the shift of the v inhibited and uninhibited nullclines at $g_{appE(max)}$.The light blue nullclines shows the shift of the v inhibited and uninhibited nullclines at $g_{appE(min)}$ 25

7 Changes in silent phase duration with changes in g_{app_1}, the drive to cell 1. In each plot, g_{app_3}, was held fixed at $\bar{g_{app}}$, the baseline drive for the corresponding model (*dotted vertical line*), and g_{app_1} was varied above and below that level. T_{s_1} and T_{s_3} denote the resulting silent phase durations of cells 1 and 3, respectively, and T_{s_0} (*dotted horizontal line*) denotes the silent phase duration with $g_{app_1} = g_{app_3} = \bar{g_{app}}$. Half-center oscillations based on persistent sodium current tuned to E-Escape 26

8 Time courses for periodic oscillations of cell 1 (black),cell 2 (red), cell 3 (green), cell 4 (blue) tuned to an inhibitory escape regime 29

9 Basic nullcline configurations and periodic orbits for the four cell network with half-center oscillation mechanism for the inhibitory escape regime.The solid lines are v-nullclines. The red cubic curves represents the inhibited v-nullclines while the blue curves represent the uninhibited v-nullcline for cells 1 and 3. For cells 2 and 4 the red cubic curves represents its unexcited v-nullclines while the blue curves represent their excited v-nullcline. The dashed green lines are slow variable nullclines, thick black lines are trajectories corresponding to half-center oscillation, and "vertical" dotted lines show synaptic threshold . . 30

10 The periods of the basic periodic orbits shown in Figure 8 vary with the drive to both cells 2 and 4. 32

11 **Nullcline variation changes of g_{appI} of inhibitory cells:** The red nullclines represents the unexcited and excited v- nullclines set at its baseline g_{appI} drive. The purple nullclines shows the shift of the v unexcited and excited nullclines at $g_{appI(max)}$.The light blue nullclines shows the shift of the v unexcited and excited nullclines at $g_{appI(min)}$ 33

12 Changes in silent phase duration with changes in g_{app_2}, the drive to cell 2. In each plot, g_{app_4}, was held fixed at g^-_{app}, the baseline drive for the corresponding model (*dotted vertical line*), and g_{app_2} was varied above and below that level. T_{s_2} and T_{s_4} denote the resulting silent phase durations of cells 2 and 4, respectively, and T_{s_0} (*dotted horizontal line*) denotes the silent phase duration with $g_{app_2} = g_{app_4} = g^-_{app}$. Half-center oscillations based on persistent sodium current tuned to I-Escape 34

13 Time courses for periodic oscillations of four cells (cell 1 (black), cell 2 (red), cell 3 (green), cell 4 (blue)) tuned to an excitatory release. 37

14 Basic nullcline configurations and periodic orbits for four cell connections with half-center oscillation mechanism for an excitatory release regime. The solid lines are v-nullclines. The red cubic curves represents the inhibited v-nullclines while the blue curves represent the uninhibited v-nullcline for cells 1 and 3. For cells 2 and 4 the red cubic curves represents its unexcited v-nullclines while the blue curves represent their excited v-nullcline. The dashed green line are slow variable nullclines, thick black line are trajectories corresponding to half-center oscillation, and dotted line shows synaptic threshold 38

15 A zoomed image of cell 1 shows us the range of possible solutions for $I_L = [h_{fP}(0), h_{LK}(s_{max})]$ that will ensure cells 1 and 3 are able to jump to the active phase in segment IV. 39

16 The periods of the basic periodic orbits shown in Figure 13 vary with changes in drive to both cells 1 and 3 40

17 **Nullcline variation changes of g_{appE} of excitatory cells:** The red nullclines represents the inhibited and uninhibited v nullclines set at its baseline g_{appE} drive. The purple nullclines shows the shift of the v inhibited and uninhibited nullclines at $g_{appE(max)}$.The light blue nullclines shows the shift of the v inhibited and uninhibited nullclines at $g_{appE(min)}$ 41

18 Changes in silent phase duration with changes in g_{app_1}, the drive to cell 1. In each plot, g_{app_3}, was held fixed at g^-_{app}, the baseline drive for the corresponding model (*dotted vertical line*), and g_{app_1} was varied above and below that level. T_{s_1} and T_{s_3} denote the resulting silent phase durations of cells 1 and 3, respectively, and T_{s_0} (*dotted horizontal line*) denotes the silent phase duration with $g_{app_1} = g_{app_3} = g^-_{app}$. Half-center oscillations based on persistent sodium current tuned to E-Release 42

19 Time courses for periodic oscillations of four cells (cell 1 (black),cell 2 (red), cell 3 (green), cell 4 (blue)) tuned to an inhibitory release. 44

20 Basic nullcline configurations and periodic orbits for four cell connections with half-center oscillation mechanism tuned to an inhibitory release regime. The solid lines are v-nullclines. The red cubic curves represents the inhibited v-nullclines while the blue curves represent the uninhibited v-nullcline for cells 1 and 3. For cells 2 and 4 the red cubic curves represents its unexcited v-nullclines while the blue curves represent their excited v-nullcline. The dashed green line are slow variable nullclines, thick black line are trajectories corresponding to half-center oscillation, and dotted line shows synaptic threshold. 45

21 Zoomed in image of cell 1 shows the range of possible solutions for $I_R = [h_{RK}(s_{min}), h_{FP}(0)]$ that will ensure cells 1 and 3 are able to jump to the silent phase in segment I. 46

22 The periods of the basic periodic orbits shown in Figure 19 vary with changes to the drive of both cells 2 and 4 47

23 **Nullcline variation changes of g_{appI} of inhibitory cells:** The red nullclines represents the excited/unexcited v-nullclines set at their baseline g_{appI} drive. The purple nullclines shows the shift of the v excited/unexcited nullclines at $g_{appI(max)}$.The light blue nullclines shows the shift of the v excited/unexcited nullclines at $g_{appI(min)}$ 48

24 Changes in silent phase duration with changes in g_{app_2}, the drive to cell 2. In each plot, g_{app_4}, was held fixed at g_{app_0}, the baseline drive for the corresponding model (*dotted vertical line*), and g_{app_2} was varied above and below that level. T_{s_2} and T_{s_4} denote the resulting silent phase durations of cells 2 and 4, respectively, and T_{s_0} (*dotted horizontal line*) denotes the silent phase duration with $g_{app_2} = g_{app_4} = g^-_{app}$. Half-center oscillations based on persistent sodium current tuned to I-Release 49

25 Time courses for periodic oscillations of four cells (cell 1 (black),cell 2 (red), cell 3 (green), cell 4 (blue)) set to an inhibitory adapt escape regime. 52

26 Basic nullcline configurations and periodic orbits for four cell connections with half-center oscillation mechanism tuned to an inhibitory adapt escape regime. The solid lines are v-nullclines. The red cubic curves represents the inhibited v-nullclines while the blue curves represent the uninhibited v-nullcline for cells 1 and 3. For cells 2 and 4 the red cubic curves represents its unexcited v-nullclines while the blue curves represent their excited v-nullcline. The dashed green line are slow variable nullclines, thick black line are trajectories corresponding to half-center oscillation, and dotted line shows synaptic threshold. 53

27 The periods of the basic periodic orbits shown in Figure 25 vary with changes in drive to both cells 2 and 4 54
28 **Nullcline variation changes of g_{appI} of inhibitory cells:** The red nullclines represents the excited/unexcited v-nullclines set at its baseline g_{appI} drive. The purple nullclines shows the shift of the v excited/unexcited nullclines at $g_{appI(max)}$.The light blue nullclines shows the shift of the v excited/unexcited nullclines at $g_{appI(min)}$ 55
29 Changes in silent phase duration with changes in g_{app_2}, the drive to cell 2. In each plot, g_{app_4}, was held fixed at g_{app_0}, the baseline drive for the corresponding model (*dotted vertical line*), and g_{app_2} was varied above and below that level. T_{s_2} and T_{s_4} denote the resulting silent phase durations of cells 2 and 4, respectively, and T_{s_0} (*dotted horizontal line*) denotes the silent phase duration with $g_{app_2} = g_{app_4} = g^{-}_{app}$. Half-center oscillations based on persistent sodium current tuned to inhibitory adapt escape. 56
30 Time courses for periodic oscillations of (cell 1 (black), cell 2 (red), cell 3 (green), cell 4 (blue)) set to an excitatory adapt release regime 58
31 Basic nullcline configurations and periodic orbits for four cell connections with half-center oscillation mechanism tuned to an excitatory adapt release regime. The solid lines are v-nullclines. The red cubic curves represents the inhibited v-nullclines while the blue curves represent the uninhibited v-nullcline for cells 1 and 3. For cells 2 and 4 the red cubic curves represents its unexcited v-nullclines while the blue curves represent their excited v-nullcline. The dashed green line are slow variable nullclines, thick black line are trajectories corresponding to half-center oscillation, and dotted line shows synaptic threshold. 59
32 The periods of the basic periodic orbits shown in Figure 30 change with changes in drive to both cells 1 and 3 61
33 **Nullcline variation changes of g_{appE} of excitatory cells:** The red nullclines represents the inhibited and uninhibited v-nullclines set at its baseline g_{appE} drive. The purple nullclines shows the shift of the v inhibited and uninhibited nullclines at $g_{appE(max)}$.The light blue nullclines shows the shift of the v inhibited and uninhibited nullclines at $g_{appE(min)}$ 62
34 Changes in silent phase duration with changes in g_{app_1}, the drive to cell 1. In each plot, g_{app_3}, was held fixed at g_{app_0}, the baseline drive for the corresponding model (dotted vertical line), and g_{app_1} was varied above and below that level. T_{s_1} and T_{s_3} denote the resulting silent phase durations of cells 1 and 3, respectively, and T_{s_0} denotes the silent phase duration with $g_{app_1} = g_{app_3} = g^{-}_{app}$. Half-center oscillations based on persistent sodium current tuned to excitatory adapt release. 63

PREFACE

First of all, I would like to express my sincere gratitude to my advisor Dr. Jonathan Rubin for his continuous support throughout the research for this thesis, for his motivation, for his immense knowledge, and for his patience. I could not have imagined having a better advisor and mentor for my M.S. study.

Besides my advisor, I would like to thank the rest of my thesis committee, Dr. Swigon and Dr. Dorion, for their insightful comments, encouragement, and for offering their time to be a part of my committee.

In particular, I am very thankful to Philippa Carter for always believing in me even when I didn't. Thank you for always giving me a lifeline and pushing me to achieve my goals.

To my fellow students who have been so supportive every step of the way. A special thanks to Emma Everett for always being there to help me with any questions and acting as an overall support through this experience. Also, I would like to thank Youngmin Park for always opening his door and answering my many inquiries.

To my parents, thank you for believing in me and pushing me to work hard and achieve my goals and dreams. Thank you for telling me every day how proud you are of me.

To my dear husband, Joseph, thank you for sharing this journey with me as we both struggled to pursue our passion for mathematics. Every difficult moment in life is possible because you are with me. Your love and commitment are my foundation and I feel very blessed to share this life with you. Finally, I want to dedicate this thesis to my little Angela. You are my motivation every day to fight hard and push through any obstacles. Thank you for being the most loving and understanding child in the world. Seeing your face at the end of every day reminds me of why it is important for me to fight for my dreams.

1.0 INTRODUCTION

Central pattern generators (CPGs) are intrinsic spinal networks found in all invertebrates. They help to control the patterns and timing of locomotor activities in mammals through a wide range of complex rhythmic coordinated muscle activities such as walking, flying, swimming, breathing, and etc.

When locomotion activities begin, CPG networks activate and become responsive to inputs from locomotor commands that come from the brain-stem and mid-brain. Once activated, CPGs are the neurons responsible for providing rhythmic activity responses. CPGs are able to generate alternating rhythmic activity of flexor and extensor interneurons that serve as the basic foundation of circuit interaction that enables locomotion activity in mammals [11, 12, 17]. While maintaining the rhythmicity of their activity, CPGs are also able to adjust their activity output as a response to inputs from higher centers and sensory feedback [36].

CPGs are sensitive to sensory feedback. Consequently, modeling CPG locomotion activities provides further insight to understanding complex neuronal networks since they produce measurable outputs that have a direct relationship with the behavior and activity of the neural network. These observations might provide further intuition into more complex behaviors of cortical network activity.[13].

The organization of locomotion in vertebrates relies on the two main functions that are carried out by CPG networks which are rhyghm generation and pattern generation. Together, they affect the period of activity and the rhythmic activation of motor neurons that allow for left-right coordination. It was observed in the neurobiology of rodents that neurons of its spinal CPGs may be divided into four different classes: rhythmogenic interneurons (RGNs), ipsilateral coordinating interneurons (ICNs) motoneurons (MNs),and commisural

interneurons (CINs)[26].

Through different experiments, we have learned that when carefully relating the firing pattern and postsynaptic effects, it is possible to understand the role of groups of rhythmogenic interneurons in the CPG [14]. The RGNs are believed to be a heterogenoeus group of interneurons which assist with rhythmic oscillatory drive that serves as a basis to the locomotor pattern. ICNs act through inhibition and enforce the alternation between extensor-associated and flexor-associated neuron groups on a single side of the midline. It was observed that motorneurons directly innervate the flexor or extensor muscles on one side of the rodent and excite muscular contraction while limiting their own firing by exciting Renshaw cells which inhibit the motorneurons[14, 26].

The muscle activity of the left and right side of the body are controlled by commissural interneurons CINs. These help the contralateral side of the cord and activate the interneurons and motorneurons to react since they coordinate activity on the two sides of the body [28]. Such connections will allow for different locomotor activities that produce a range of gaits such as walking, hopping, skipping or galloping [23].

It was found that certain CINs are composed of a mixture of glutamatergic and glycinergic pathways which allow for direct communication between flexor and extensor interneurons. CINs that fire in the extensor phase inhibit contralateral extensor and excite contralateral flexors. Some of these experimental studies have found that limbed animals have gaits that are defined by left-right leg coordination and speed during which the coordination of the left right motion activities are controlled in the spinal chord through CINs [15]. Therefore, it was suggested that CINs are responsible for fine tuning the motion and coordinating motor neuron activity by providing a direct input to the interneurons on the contralateral side with inhibitory and excitatory inputs. Also, when CINs were significantly reduced, they allowed for a synchronous respons of left right coordination during fictive locomotion [20].

Therefore, CINs are important factors in CPG locomotion due to their role in the left-right locomotion activity in correlation to results observed in turtle activity (Stein 1995)[31] and cat hind-limb movement (Ivashko 2002)[10]. However, other studies have suggested that CINs are not the only source involved in rhythmic activity because the rhythm can be induced in rodents and cats (Nishimaru 2006)[19]. Other models have also studied the

rodent and cat spinal cord through classical modeling of spinal motor function. They have demonstrated that the cat spinal cord was able to generate a locomotor rhythm of alternating contractions in ankle flexors and extensors in the absence of input from higher centers and afferent feedback [2] However, overall it has been shown that when only one side of the cord is active, the period of locomotor activity is not only significantly longer, but the amplitude is relatively unchanged (Kjareluff and Kiehn 1997)[15].

Shevstova et al. [29] suggested two different computational models of spinal locomotor circuits consisting of left and right rhythm generators which interacted bilaterally through neuronal pathways mediated by different excitatory and inhibitory CIN populations. The study provided some insight into the architecture and organization of spinal networks as well as the connectivity of the inhibitory and excitatory CIN pathways that maintain alternating and synchronous rhythmic activity. The models suggested a representation of symmetric bilateral networks of neural population of left and right rhythm generating networks with flexor and extensor centers and inhibitory-excitatory interneuron interactions between them.

It has also been well studied that excitatory and inhibitory cells are present in the mammalian spinal cord. Inhibitory cells facilitate mutual inhibition and promote alternating activity. Excitatory cells provide an excitatory input to contralateral neurons by helping synchronize activity or promoting mutual inhibition of left-right alternation by acting via inhibitory interneurons situated on both sides of the spinal cord [5, 23].

While it is clear that mammalian CPG neural activity is complex, different research has proven that we can still have a basic understanding of its network interactions and the different components that produce rhythmic activity responses. The flexibility and adaptability of CPGs help adjust the oscillatory patterns, as well as their frequency and phase durations, which are necessary to model the organismal demands and locomotion that rely on the different excitatory and inhibitory inputs.

Brown [3] proposed that CPGs could be represented through a half-center model which matched the ideas of how these spinal interneurons worked in mammalian locomotion activities. A half-center oscillator is a common circuit building block of CPG networks. These networks are composed of interneurons that could control flexor and extensor motorneurons that produce rhythmic motor patterns through reciprocal inhibitory connections and are

capable of sustaining alternating activity. These type of neural interactions controlled by inhibitory neurons in the spinal cord were widely observed in the motor coordination that were produced in newborn mice in vitro. It was observed that through synaptic transmissions from interneurons, synchronization of flexor and extensor motorbursts were produced [36].

The premise of the modeling suggested that each limb is controlled by a separate group of CPGs and each group is composed of, excitatory interneurons and mutually inhibitory interconnections between the half centers. Thus, each group alternates between active and silent states with only one active half-center at a time. The jump from active to silent phase occurs when there exists a reduced level of excitability of one of the half-centers. Once the excitability level of the active half-center falls below a threshold, it becomes silent and allows for the opposing center to activate in return [12, 3]. Half center oscillators have been found to affect the timing in which motor patterns are controlled by pairs of reciprocally inhibitory neural pairs or networks in motions such as the leech heartbeat or the tadpole swimming [6, 34]. In particular, a study of cats with chronic thoracic spinal lesions displayed different speeds for left and right hindlimbs while stepping on a split treadmill. While on normal or treadmill locomotion, the shortening of the step cycle through the shortening of the extensor phase was still able to maintain the flexor phase at a relative constant rate. The study found that gait of locomotion is critically controlled by the rhythmic patterns of the CPG when directing each limb through rhythmic patterns to either extensor or flexor phases even in the absence of afferent feedback [35].

It has been observed in rodents that through *in vivo* and *in vitro* experiments of normal locomotion that while one side of the flexor muscle of an animal is active, it is out of phase with the flexor muscle of the other side. Yet, there is a similar cross-cord alternation of the extensor muscle activity. Also, while the flexor muscles of one side of the animal are active, they are anti-phase with the extensor muscles with which they are coupled [5, 4]. Sherwood et al. [26] describe this as simultaneous ipsilateral flexor-extensor antisynchrony and contralateral flexor-extensor synchrony.

Early theoretical research on half-center oscillators found that the inhibitory connections of two neurons or neuron networks can produce rhythmic alternating responses (oscillatory

or bursting) regardless of whether the individual network was capable of bursting on its own [2]. This behavior was found to exist on neurons that, through some time-dependent process, could overcome inhibition it received from an active neuron.

Wang and Rinzel were one the first to study and provide a detailed explanation of these different network connection mechanisms [33]. They found how these could help create oscillatory responses when coupling networks of two-cell connection through reciprocal inhibition. When they modeled the connections with the activation of leak conductance and a synaptic current, they were able to get the desired response due to the innate behavior of post inhibitory excitation and presynaptic voltage of each current.

Skinner et al. [30] extended the study of Wang and Rinzel [33], proposing that a thorough understanding of CPGs must also provide insight into the understanding of their response to different inputs. Through modeling mechanisms using Morris-Lecar type cells, they proposed four different mechanisms that lead to oscillatory response of active and silent phases in networks of two reciprocally inhibitory cells. Two of the mechanisms dealt with the intrinsic properties of the neurons and the other two studied the synaptic properties of the neurons, each one producing responses of "release" and "escape" [30]. Therefore, rhythmic motor behaviors produced by CPGs can produce an output that critically depends on the interactions of both synaptic and intrinsic conductance of the neurons within their networks.

Coupled neurons that are able to generate an oscillatory response based on escape and release mechanisms transition between active and silent phases in anti-phase during rhythmic activity. Escape mechanism occurs when the silent cell is able to overcome the inhibition it is receiving from its coupled cell and therefore enters the active phase. The release mechanism on the other hand occurs when the active cell transitions from the active phase to a silent phase releasing its coupled inhibited cell. However, it has been shown that to better understand this interaction of oscillatory responses to input, it is important to thoroughly study the phase plane curves that measure the phase shift of a cell in response to any input as a function of time [24, 36]. Networks coupled through half-center oscillations are strongly modulated by different inputs that affect the synaptic strengths and intrinsic properties of the neurons .

To further understand half-center CPG models, it was necessary to understand how the symmetric networks linked through reciprocal inhibition and worked in conjunction with the variation of the cellular intrinsic properties. While a locomotor rhythmic output may be considered as an oscillatroy behavior emergent from network interactions, it is possible that intrinsic properties of bursting interneurons also play a role in rhythmic behavior.

Neuron populations in adult mice displayed different types of connections of neural networking, predominantly in the spinal cord through embryonic neurons. Ryback [23] proposed a reduced model of bilateral spinal circuits based on a previous model of Zhong et al. [37] simulating neural connectivity of genetically induced reorganization of spinal cord and its functionality in controlling responses in locomotor gaits of mice. The model suggests a bilateral symmetric network interaction between two intrinsically rhythmic neural populations of left and right coordination and rhythm-generating flexor centers. Such rhythmicity was activated by a persistent sodium current (I_{Nap}) in each neuron along with an excitatory synaptic interaction.

Recent models of spinal circuits and CPG locomotor activity attempt to simulate the interactions of pools of tens or hundreds of spiking neurons. These spiking neurons are modeled via Hodgkin-Huxley style and are described by five to ten differential equations per neuron.[18, 21, 23, 27, 37]. Due to these complex connections, these large networks become too difficult to analyze mathematically. Other studies found that some simplifications would be useful.

When analyzing different CPG models such as mammalian respiratory CPG [21, 22] it was found that by using the average voltage for one spiking neuron that representing a population of spiking neurons can notably simplify the analysis. This simplification can also provide insight into the transitions between silent and active states within the dynamics of the neural population. Another simplified model that explored CPG interactions through half-center coordinations has been presented by Daun et al. [8]. They studied the asymmetry of the response in flexor-extensor phase durations that was achieved through the changes in drives of the half-center simulations of two interacting neurons. They proposed using different models to describe different mechanisms. Slowly inactivating persistent sodium current to model escape, adaptation based on a calcium-dependent potassium current, and post-

inhibitory rebound excitation calcium current to model release were used. It was observed that the slowly persistent sodium current showed the greatest range of oscillatory periods and also the greatest degree of freedom in phase duration while controlling asymmetric inputs to the network.

However, while simplification of the model can be very useful, it is important to consider possible limitations of different methods based on the original structuring of half-centers. One of these may be that some simplified models consider only one pattern of alternation between on set of flexor-extensor or left-right activity. This forces all interacting CPG neurons to be separated into only one of these two groups. Other limitations to keep in mind are that in some models only one half-center body can produce alternating activity with only one burst per cycle to either coordination of flexor-extensor or left-right pairs. Therefore, it becomes difficult to find two bursts per cycle that have been observed by some motoneurons during some locomotion activity.[7]. Some suggestions have been made to investigate more complex network interactions that may provide further insight into different architectures of half-center connections while maintaining some of the necessary simplifications that will help us mathematically analyze results.

Molkov et al.[18] proposed using simplifications of neural connectivity, as those proposed by Rubin et al. [21], while trying to maintain a biophysical accuracy of locomotion activity. They established that using similar simplifications as those described above can help reduce a large scale model for computer simulations of spinal circuits of CIN mediated interactions. However, they considered four pacemaker neurons representing left and right, flexor and extensor rhythm-generating centers interacting via commissural pathways. Their model was able to generate busting activity through a range of different parameters of neuronal excitation and burst frequencies showing a change of burst amplitude as frequency increased. This suggests an explanation for different experimental studies.

Thus, keeping in mind the benefits of adding a more biologically relevant architecture to a network, we will consider the governing equations similar to the persistent sodium model proposed by Daun et al. [8]. This particular model was chosen due to the fact that the persistent sodium based network exhibited the greatest range of oscillation periods and the greatest degree of independence in phase duration control by asymmetric inputs within

its regime. Therefore, following similar numerical simulations and phase-plane analysis as Daunt et al.[8] we want to investigate if similar results are achieved when modifying the architecture of Daun et al. [8] proposed two cell model network to a Molkov-like network [18]. However, while we propose a reduced four neuronal population network, we will be omitting CIN interactions in order to check how any additional excitatory-inhibitory interactions may affect the responsiveness of the oscillatory activity to variations to the external applied drive.

Our model is based on rhythm-generating neural circuits which will help us study the interaction between four neuron cells coupled in pairs of inhibitory and excitatory activities produced by two pairs of symmetrically constructed neural populations. These cross-cord connections contain a contra-lateral excitatory-excitatory and inhibitory-inhibitory network connection through inhibitory interneurons as well as excitatory-inhibitory ipsilateral excitations. We will consider the intrinsic properties of the acting interneurons. Also, we look into the effects of applied currents coupled through a wider range of synaptic inputs as well as neuromodulation will contribute to the rhythmicity of the network are considered.

Our main focus will be studying the oscillatory responses through different mechanisms of escape and release from one general model. This is achieved through different parameter adjustment that define the various phase planes of nullcline configurations for each regime. Using a range of external drive input to the half-centers, we were able to show that the frequency is strongly dependent of the different models proposed throughout this study.

The thesis is organized as follows. Chapter 2 will introduce the general model for our 4 cell network and the dynamics of the system along with the equations that represent it. This chapter also describes the approaches used to study the changes of oscillatory period and phase durations due to symmetric and asymmetric perturbations of the applied external drive. Chapters 3 and 4 describe the different mechanisms of intrinsic escape and release respectively. Chapter 5 explores different escape and release mechanism under the adaptation of the synaptic input. Finally, chapter 6 provides the conclusion of each method through a discussion and comparison of all oscillatory and phase responses throughout all the prescribed regimes.

2.0 METHODS

2.1 CPG MODEL

As previously mentioned in chapter 1, foregoing theoretical research has shown that half-center oscillations can be achieved through different intrinsic and synaptic network mechanisms. [9, 16, 30, 33]. In particular, Skinner et al. proposed a model of two half-centered coupled cells that produced half-center oscillations through mutual reciprocal inhibition even when the uncoupled cells were not oscillatory themselves. The output of oscillatory responses occurred when the activity of each half-center was experiencing some form of adaptation through the coupling of the two cells. Through this coupling, they described four different mechanisms. Two considered the intrinsic mechanisms of escape and release. The other two cases consider the contribution of the synaptic threshold voltage giving place to mechanisms of synaptic release and synaptic escape.

The structure of the network proposed for this study is modeled by half-center oscillators of spinal CPG networks in which connections of activations and inhibition of tonically or oscillatory spiking neurons will result in bursts with alternating rhythm produced by an escape or release mechanism. These mechanisms emerge due to the dynamics of persistent sodium current (I_{Nap}) for each half center oscillator and the different inputs of excitation and inhibition between them. The model proposed by Daun et al. [8] considered two neurons with mutually inhibitory synaptic connections. The analysis they proposed was based on perturbations to the excitatory external drive to one or both neurons and how these produced changes in burst amplitude and frequency in the oscillatory responses of the network.

Our study will build upon the model and analysis proposed by Daun et al. [8]. However, we will now be considering a four cell model that is designed to help bridge the gap between an

abstract two cell models into a more biophysically realistic model of oscillatory neurons that are synaptically coupled. With these newly constructed connections, we want to determine if the more our new model configuration will change the dynamics of the network and impact the range of oscillatory responses through any changes in burst amplitude and frequency.

Our model represents the connections of spinal circuits through a bilateral symmetric network of neural populations. The model considers excitatory and inhibitory connections between two pairs of left-right or flexor-extensor centers of rhythm generating networks. Thus, in our architecture, we simplify the neuronal organization of the networks in the spinal cord to two functional classes: inhibitory and excitatory. Our network will be composed of two intrinsically excitatory neural populations which will be referred to as cell 1 and cell 3, and two intrinsically inhibitory neural populations which will be referred to as cell 2 and cell 4.

The construction of our model considers a four cell lateral cross-cord connection that includes an ipsilateral excitatory-inhibitory excitation as well as a contra-lateral inhibitory-excitatory inhibition Figure 1. It is similar to cross-cord connections studied for flexor-extensor models [5, 26]. However, this four cell network can be paired as flexor (cells 1 and 3) and extensor (cells 2 and 4) or left (cells 1 and 2) and right (cells 3 and 4) neurons that mutually inhibit each other through inhibitory interneurons and synaptic connections that form a regime of half-center oscillations.

The oscillatory solutions consist of two phases for which one excitatory and inhibitory cell become coupled in active and silent phase trajectory. We will consider that two neurons will be in the active phase simultaneously (e.g. cells 1 and 2 or cells 3 and 4) while the other set of neurons is simultaneously in the silent phase (e.g. cells 3 and 4 or cells 1 and 2). Due to the fast dynamics of the system, all cells will experience a rapid transitions between silent and active phases almost at the same time. Thus, through computer simulations of the network, we will study the changes of oscillatory patterns that depend on the fine tuning of current drives and strengths of synaptic connections between the cells.

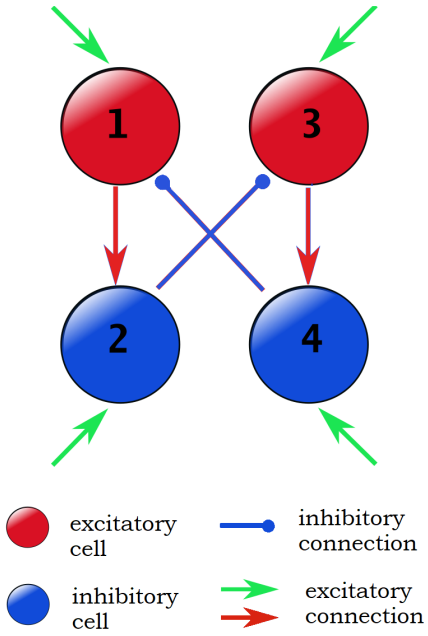

Figure 1: **Organization of locomotor CPG's.** Schematic of interactions between the locomotor half-centers. The rhythm generator pairs consist of intrinsically excitatory cells (1 and 3) and intrinsically inhibitory cells (2 and 4).

2.2 COMPUTATIONAL MODEL EQUATIONS

All cells are structured under a conductance-based Hodgkin-Huxley style and consider the persistent sodium current (I_{NaP}) with slow inactivation as a source of oscillations. This model is able to produce bursting and oscillatory activity through a wide range of parameter changes that define neural excitation and burst frequency while exhibiting changes of burst amplitude and frequency. Based on Rubin et al models[21, 22], each cell is represented by a system of ordinary differential equations.

For cells $j \in \{1, 4\}$ and $k = ((j + 2) \bmod_4 + 1)$, consider:

$$C_m v_j' = -I_{Nap}(v_j, h_j) - I_L(v_j) - I_{syn}(v_j, s_k) - I_{app}(v_j), \tag{2.1}$$

where C_m is the capacitance of the membrane with units $\mu\text{F/cm}^2$. Here, $v_j(t)$ is voltage or potential of each cell membrane individually, whose derivative is $v'(j) = dv/dt$ for t representing time. Here, s_k modulates the strength of the coupling of the synaptic current between cells j and k. The monotone sigmoidal functions $h_\infty(v)$ decrease with respect to v while $m_\infty(v)$ and $s_\infty(v)$ increase with respect to v. In this case, $h_\infty(v)$ is the steady state of the inactivation gating variable and $m_\infty(v)$ is the voltage-dependent steady state of the persistent sodium current activation. Also, $s_\infty(v)$ is the level of activation of the synapses and takes values between $[0, 1]$. These functions are defined as

$$h'_j = (h_\infty(v_j) - h_j)/\tau_h(v_j), \tag{2.2}$$

$$s'_j = \alpha \cdot s_\infty(v_j)(1 - s_j) - \beta s_j, \tag{2.3}$$

$$m_\infty(v) = 1/(1 + \exp((v - \theta_m)/\sigma_m)), \tag{2.4}$$

$$s_\infty(v) = 1/(1 + \exp((v - \theta_s)/\sigma_s)),\ \sigma_s > 0, \tag{2.5}$$

with a limiting case of $s_\infty(v) = H(v)$, the Heaviside step function, as $\sigma_s \downarrow 0$. Maintaining $\sigma_s \downarrow 0$ implies that the trajectories $f(v, h) = 0$ stay close to the nullcline until they reach a local maximum or minimum, in which case, they are able to quickly transition to another branch through an instantaneous jump. Moreover, $\tau_h(v)$ is the time constant with respect to v and we define it as

$$\tau_h(v) = \epsilon \cosh((v - \theta_h)/\sigma_h/2). \tag{2.6}$$

In equations (2.4), (2.5) and (2.6), θ_x and σ_x for $x \in \{\text{s,m,h}\}$ represent the gating variable's half activation voltage and slope, respectively. The membrane currents described in equation (2.1) have the form

$$I_{NaP}(v, h) = g_{nap} m_\infty(v) h(v - e_{na}),$$

$$I_L(v) = g_l(v - e_l),$$

$$I_{syn}(v_j, s_k) = g_{syn} s_k (v_j - e_{syn}),$$

$$I_{app} = g_{app}(v_j - e_{app}).$$

Equation(2.1) describes the change of voltage through the membrane of each cell in terms of its inscribed persistent sodium (I_{NaP}), leak (I_L), synaptic (I_{syn}) and applied (I_{app}) currents. In this case (I_{app}) maintains $g_{app} > 0$. Altogether these currents can produce a change in the membrane potential of each cell.

Here g_{nap}, g_l, g_{syn} and g_{app} are the maximal conductances ans e_{nap}, e_l, e_{syn} and e_{app} are reversal potentials belong to the sodium, leak, synaptic and applied currents, respectively. Note that s corresponds to the synaptic input received by each cell that is driven by the voltage of its paired cell through the (I_{syn}) current. The (I_{app}) current is also treated as synaptic but is independent of other cells in the network.

Note that $g_{syn} s_k > 0$ and thus when the regimes where the dynamics of the system are driven by the inhibitory input, we have that $v_j > e_{syn}$ and therefore $v_j' < 0$ for most of the relevant values. However, if the system is driven by the excitatory input, we have that $v_j < e_{syn}$ for almost all of the relevant values v_j and therefore $v'j > 0$ for most values in the excitatory cases.

Denote the interval for $I_s := [0, \alpha/(\alpha + \beta)]$ which is positively invariant for s such that

$$s_{max} := \frac{\alpha}{\alpha + \beta}.$$

For all the methods used throughout, there are particular sets of parameters that remaining constant. See Table 1.

Geometric phase plane analysis is utilized and allows for a deeper understanding into the properties of solutions. The phase plane for the system of v and h nullclines will help us analyze the behavior of different model regimes under different combinations of parameter inputs. Similar assumptions are considered as in Daun et al.[8] and adapted to our models as follows:

Let $j \in \{1, ..., 4\}$ and fixed $s_k \in I_s$, the v-nullcline where $\{(v_j, h_j) : F_i(v_j, h_j, s_k) = 0\}$, we get a cubic shaped curve with left, middle and right branches seen in the (v_j, h_j) phase plane.

Parameters	Values	Parameters	Values
β	1	C_m	0.21
e_{na_E}	50.0	e_{na_I}	50.0
e_{l_E}	- 65.0	e_{l_I}	- 65.0
e_{syn_E}	10.0	e_{syn_I}	- 80.0
e_{app_E}	0.0	e_{app_I}	0.0

Table 1: These parameters are set constants through all the different mechanisms studied. Each subscript has an E or I description that stands for excitatory or inhibitory corresponding to the intrinsic nature of the cell they correspond to.

We can now drop the subscript for s_k for simplicity and consider the branches of $F_i = 0$ were for a fixed $s \in I_s$ there exists left, middle and right branches of their nullclines. All three defined functions are set up as $V_{L_i}(h, s) < V_{M_i}(h, s) < V_{R_i}(h, s)$ where $i \in I, E$, which correspond to inhibitory and excitatory cells, respectively.

Let $j \in \{1, ..., 4\}$, the h-nullcline $\{(v_j, h_j) : g_j(v_j, h_j) = 0\}$ is a monotone curve in the (v_j, h_j) plane that intersects $F_j = 0$ at a *unique* point $P_{FP}(0) = (v_{FP}(0), h_{FP}(0))$.

All solutions are attracted toward the left and right branches of the v-nullcline since h is a slow activating function. Depending on different parameter regimes, there can be different attracting points where the two nullclines intersect and yield a rest state for the cell. The meeting points $P_{FP}(0)$ between both v and h nullclines will give us information about the intrinsic behavior of the uncoupled cell. Thus, we consider a cell whose $P_{FP}(0)$ is on the hyperpolarized left-most branch of the v-nullcline to be intrinsically excitable. A cell whose $P_{FP}(0)$ is on the middle branch is said to be intrinsically oscillatory. Finally, a cell whose $P_{FP}(0)$ lies on the depolarized right-most branch v-nullcline is said to be tonic as shown in 2a below.

Note that we consider the intersecting points $P_{FP}(0)$ on the blue uninhibited (excited for inhibitory cells) v-nullcline to determine the intrinsic behavior of the cell. Also, note

that there exist stable critical points if the nullclines intersect at the left or right knees of the v-nullcline. Bursting solutions alternate between silent phases of low voltage and active phases of spikes through rapid oscillations of different amplitude depending on the different mechanisms. We will consider phases I and III to be transition phases from silent to active and vice-versa, while phases II and IV will be either the active or silent phases of where the solution of each cell depending on the regime in which they exist. 2b

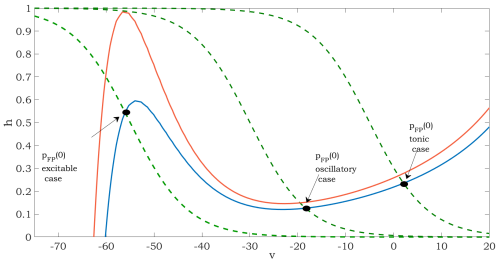

(a) Nullcline configurations illustrated in the persistent sodium model. Three different h-nullclines (*dashed* green) corresponding to $\theta_h = -5$ (excitable case), $\theta_h = -30$ (oscillatory case), and $\theta_h = -55$ (tonic case). Also shown are the inhibitory (*red*) and uninhibited (*blue*) v-nullclines

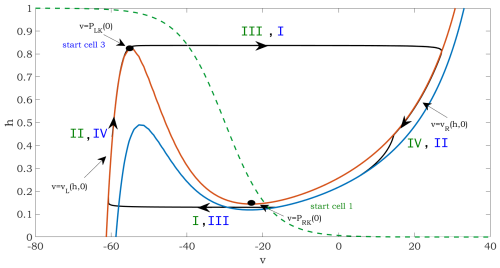

(b) We used as a model the trajectories of the excitatory cells in the e-escape regime. We color coded the trajectory of cell 1 in green and cell 3 in blue as they transition through the different phases of the solution. The inhibitory (unexcited for inhibitory cells) nullcline is colored in red while to uninhibitory (excited for inhibitory cells) nullcline is colored in blue. The thick arrows of the solution point towards the direction the cells follow. Note $vi \approx v_{L,R}(h,s)$ are the left and right branches of the v-nullcline and $P_{L,R}K(0)$ are the left and right points of equilibrium

The positions and slopes of the nullclines will define the behavior of the trajectories in the phase plane and will define the different mechanisms (escape, release, adapt) that will be analyzed. While the v-nullcline of an uncoupled cell is cubic-shaped, we will see that for large enough drives its figure will be a monotonically increasing slope, and may alter its location including the position of the knees and its overall shape when coupled. On the other hand, the h-nullcline is independent of the input of any other cell. However, we may change some parameters to alter its slope in order to achieve the mechanism that is needed. All nullcline figures of escape, release and adapt surfaces were generated based on locations of knees of appropriate v and h nullclines. They were obtained by using the software platform XPPAUT [1].

2.3 ANALYSIS OF CONTROL OF HALF-CENTER OSCILLATIONS AND PHASE DURATION

We take into consideration the period of oscillatory responses through which the CPG model can maintain its regime as we increase or decrease the applied drive through a range of values. The applied drive, denoted as g_{app_i} for $i \in I, E$, that will change will be based on whether the cells that are driving the mechanism are intrinsically excitatory or inhibitory throughout the different model regimes. In models where the dynamics of the system are initiated by intrinsically excitatory cells, g_{app_E} drive will be changed for cells 1 and 3 while maintaining g_{app_I} drive of cells 2 and 4 constant. On the other hand if the dynamics of the system is initiated by intrinsically inhibitory cells, then we will vary the g_{app_I} drive of cells 2 and 4 while maintaining g_{app_E} drive of cells 1 and 3 constant. For the analysis, we sill consider two different cases:

The symmetric case occurs when g_{app_i} for $i \in I, E$ is the same for both driving cells of inhibitory or excitatory nature. The applied g_{app_i} for $i \in I, E$ drive that varies will depend on the nature of the model analyzed.

First, we vary both drives through a range of values of g_{app_I} and g_{app_E} seeking the range of periodic solutions that will continue to yield both oscillatory responses while staying within the regime of the model analyzed. Through this range we are able to find a midpoint for the cells that are instigating the phase transitions and those which will remain constant. However, we must consider that the midpoint of the cells that will remain constant may vary at the max and min points of the range of the drive of the cells that are varied. Therefore, we take an average of the different midpoints that may exist and use this value as our overall midpoint value.

This midpoint for both excitatory and inhibitory cells which will be denoted as $g_{a\bar{p}p_E}$ and $g_{a\bar{p}p_I}$ and will be referred to as the *baseline drive*. Next, we benchmark a voltage threshold of -40 mV that is used to determine the range of onset and offset times when a cell is active. The period of active duration is denoted as $T(g_{app})$ and is normalized with the period of active duration $\bar{T}$ that is obtained with $g_{a\bar{p}p_i}$ for $i \in I, E$. This, will allow us to study the activity patterns of each model. Note that for example if we are in a model where the

excitatory cells drive the dynamics we maintain $g_{a\bar{p}p_I}$ constant, where *drive cell 2 = drive cell 4* and vary the g_{app_E} drive, where *drive cell 1 = drive cell 3*. Moreover, the change of g_{app_E} in relation to the range of the total divided by $g_{a\bar{p}p_E}$ gives us the relative T period of the system so that $\Delta T/\Delta g_{app_E}$ is the relative change of T compared to the relative range of g_{app_E}.

The asymmetric case will be analyzed using the values of *baseline drive* found in the previous case for all cells. Thus, we begin by setting all $g_{a\bar{p}p_i}$ for $i \in I, E$ and considering once again the nature of the cells that initiate the dynamics of the model, we will vary the drive of only one of either excitatory or inhibitory initiating cells while maintaining the others constant. Next, we benchmark a voltage threshold of -40 mV that is used to determine the range of onset and offset times when both driving cells are active. The period of active duration is denoted as $T(g_{app})$ for both driving cells and is normalized with the period of active duration $\bar{T}$ for both driving cells that is obtained when $g_{a\bar{p}p_I}$ for $i \in I, E$. This will allow us to study the active patterns and interactions between the periodic responses of the driving cells that initiate the dynamics of the system. Note that if we are in a model where the inhibitory cells drive the dynamics, we maintain $g_{a\bar{p}p_E}$ constant where *drive cell 1 = drive cell 3*. Next, we can arbitrarily choose cell 2 to have a varying g_{app_I} drive, where *drive cell 2* $\neq$ *drive cell 4* and the drive of cell 4 is set at $g_{a\bar{p}p_I}$.

3.0 ESCAPE MODEL

As mentioned in **Chapter 2**, oscillatory responses can occur in systems governed by a fast and slow variable. Our fast variable is given by the voltage v and our slow variable is governed by h. When coupling cells through half-center oscillators, we found that when two ipsilateral cells (e.g. 1 and 2) are silent then the other pair of ipsilateral cells (e.g 3 and 4) are active, where cell 3 actively excites cell 4 which in turn actively inhibits cell 1. Moreover, we can have an oscillatory response to the network interactions as illustrated in Figure 2 and Figure 8 based on the model shown in Figure 1. This gives way to the different dynamics of the system and their position within the different phases of the nullclines. Two different mechanisms of state transitions have been studied [30, 33] known as *release* and *escape*.

The *escape* mechanism occurs when an inhibited cell can escape from a hyperpolarized state because the left knee of its v-nullcline has no stable steady state even when the other cell is active. The silent cell can transition to an active phase since it is able to access or overtake the left knee of its v-nullcline. This mechanism can occur due to the intrinsic properties of the cell or as a result of decaying inhibition to the silent cell, depending on parameter selection. Therefore, the silent cell is able to move to an active state regardless of inhibition it may receive and thus *escapes* from inhibition. However, in a 4 cell model we also consider the case where the silent cell that is governed by the inhibited nullcline is able to transition to the uninhibited nullcline and become active. Thus, we can deduce that it is able to *escape* its trajectory through its inhibited nullcline. In return, when it crosses the synaptic threshold, it begins to inhibit or actively excite its coupled cell depending on whether it is an inhibitory or excitatory cell. This causes the formerly active cell to change from active to silent. Note that if inhibition decays before its coupled cell can escape, this is no longer considered intrinsic escape but rather escape through adaptation see **Chapter 5**.

3.1 EXCITATORY ESCAPE MODEL

3.1.1 Half-center oscillation mechanisms

The construction of periodic singular solutions for both pairs of identically coupled cells, as shown in the Figure 1, are modified to fit the regimes where the excitatory cells are the ones that instigate the dynamics within the escape model. Each pair of inhibitory and excitatory cells are under the influence of different parametric values, as seen in Table 2, with the governed dynamics described in **Chapter 2**. However, this model is adjusted to allow the excitatory cells 1 and 3 to drive the transition between the silent and active phases while instigating the same transitions for cells 2 and 4. Figure 3 shows the nullcline configuration of the baseline drive with the solution of its basic periodic orbit for each of the four cells tuned to an excitatory escape regime. In the absence of coupling, each of the cells is tonically active.

3.1.1.1 Parameters The parameter values sustaining the excitatory escape model are given by $\alpha = 3$ and the following table Table 2.

In Figure 2 we can see that cells 1 and 2, and cells 3 and 4, are both active and silent almost precisely at the same time. Thus, all 4 cells are interacting and maintaining the excitatory driven escape regime while maintaining continuous oscillatory solutions.

Oscillatory responses of the dynamics of the network when tuned to the previously mentioned parameters are illustrated in the figure above. Clearly, cell 1 and cell 2 transition from active to silent phases simultaneously and cells 3 and 4 make the phase transitions together as well. However, it is important to perform a phase plane analysis of the nullclines corresponding to the trajectory of the solution for all four cells.

The phase plane of the nullclines is clearly illustrated in Figure 3 for all four cells. In particular, we note the trajectory of the solution for all four cells with their corresponding uninhibited/excited v-nullcline in blue and inhibited/unexcited nullcline in red. The dotted vertical line shows our baseline drive for the synaptic drive $\theta_{syn_E} = \theta_{syn_I} = -43$. Also, we consider the existence of a singular periodic orbit where the limit as $\phi_s \downarrow 0$ in Equation 2.5

Excitatory cells	Values	Inhibitory cells	Values
g_{nap_E}	15.0	g_{nap_I}	4.0
g_{l_E}	2.5	g_{l_I}	3.5
g_{syn_E}	0.5	g_{syn_I}	2
$g_{app_{1,3}}$	0.275	$g_{app_{2,4}}$	0.1
θ_{m_E}	- 30.0	θ_{m_I}	-33.0
σ_{m_E}	-6.0	σ_{m_I}	-6.0
θ_{h_E}	- 30.0	θ_{h_I}	-34.0
σ_{h_E}	6.0	σ_{h_I}	6.0
θ_{syn_E}	- 43.0	θ_{syn_I}	-43.0
σ_{syn_E}	-0.1	σ_{syn_I}	-0.1

Table 2: Parameters are considered to maintain a regime of intrinsic excitatory escape model.

which helps maintaining solutions close the these $f(v, h)$ nullclines as was further explained in **Chapter 2**.

The projection of the solution of cells 1 and 3 lie on the inhibited nullcline in red. With this in mind, we will begin our phase cycle such that cell 1 and cell 2 are in the active state of the trajectory as pointed by the arrows labeled *start cell 1* and *start cell 2* in Figure 3. This will be our starting point and will follow the dynamics seen in Figure 1. Cell 1, which is positioned close to the right knee of its uninhibited blue nullcline in Figure 3, actively exciting cell 2, which is also on the blue excited nullcline. In return, cell 2 is inhibiting cell 3, which is on the red inhibited nullcline shown by the arrow. Consequently, since cell 3 has no fixed point at $v_{L_E}((h_1, 0), h_1)$, it crosses the synaptic threshold denoted by the *vertical* dotted line. Cell 3 is able to *escape* inhibition from cell 2 and begins exciting cell 4.

Cell 4 now crosses its synaptic threshold and begins to inhibit cell 1. Now, cell 1 needs to move to its inhibited nullcline but since it is below the knee of the red inhibited nullcline,

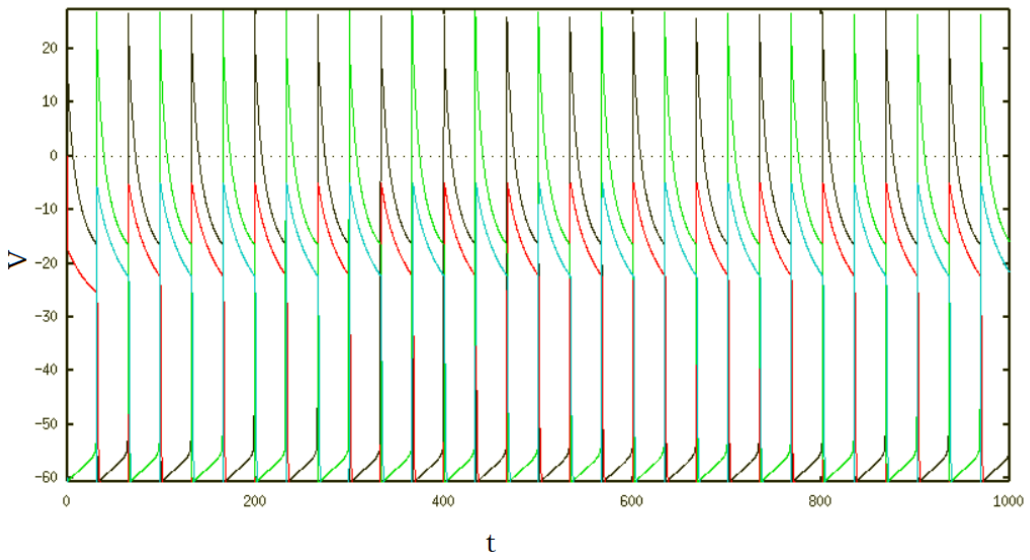

Figure 2: Time courses for periodic oscillations of four cells (cell 1 (black), cell 2 (red), cell 3 (green), cell 4 (blue)) tuned to an excitatory escape regime.

it must jump to its hyperpolarized left branch. Once it crosses the synaptic threshold it stops exciting cell 2, which is now also moving along phase I. Once cell 2 crosses its synaptic threshold, it stops inhibiting cell 3 altogether. When this happens cell 3, that is now currently in phase II, makes a "jump" in its trajectory from its red inhibited nullcline to the blue uninhibited nullcline. Cell 2 now reaches its unexcited nullcline as well. At this point, cell 1 and cell 3 have switched initial positions as have cells 2 and 4. Therefore, cell 1 and 2 are now silent and cells 3 and 4 are active. This completes half of the cycle where cells have gone through phases I and II. Repeating the same process with the new cell positions, will finish the entire cycle and bring all cells back to their original positions.

The trajectories of cells 1 and 3 must transition from the silent phase to the active phase from the left knee of the inhibited nullcline and eventually descend through the silent phase toward a fixed point which will remain above $h_{FP}(0)$. Hence, any h-values that are below $h_{FP}(0)$ will not be accessible to their trajectories. Also, note that cell 1 and cell 3 will jump down to the silent phase only if their trajectory is bellow the right knee of

the red inhibited nullcline. This will happen only if $h_E < h_{RK(S_{max})}$. Therefore, if we let $I_R = [h_{fP}(0), h_{RK}(s_{max})]$, any $h_E \in I_R$ will ensure that the inhibited cell will depolarize above its synaptic threshold and transition to its active phase. See Figure 4.

Due to the membrane potential v_j of cell 1 at the starting points, is more positive than the inhibition of the synaptic threshold as it excites cell 2, and release becomes impossible (Similarly for cells 3 and 4 in phase III). The trajectory of cells 2 and 4 are constrained to the left branch of the unexcited nullcline until their excitatory paired cells reach their synaptic threshold and rapidly excite them, providing them with enough voltage to transition to their excited nullcline and become active themselves along with their ipsilateral cell companion.

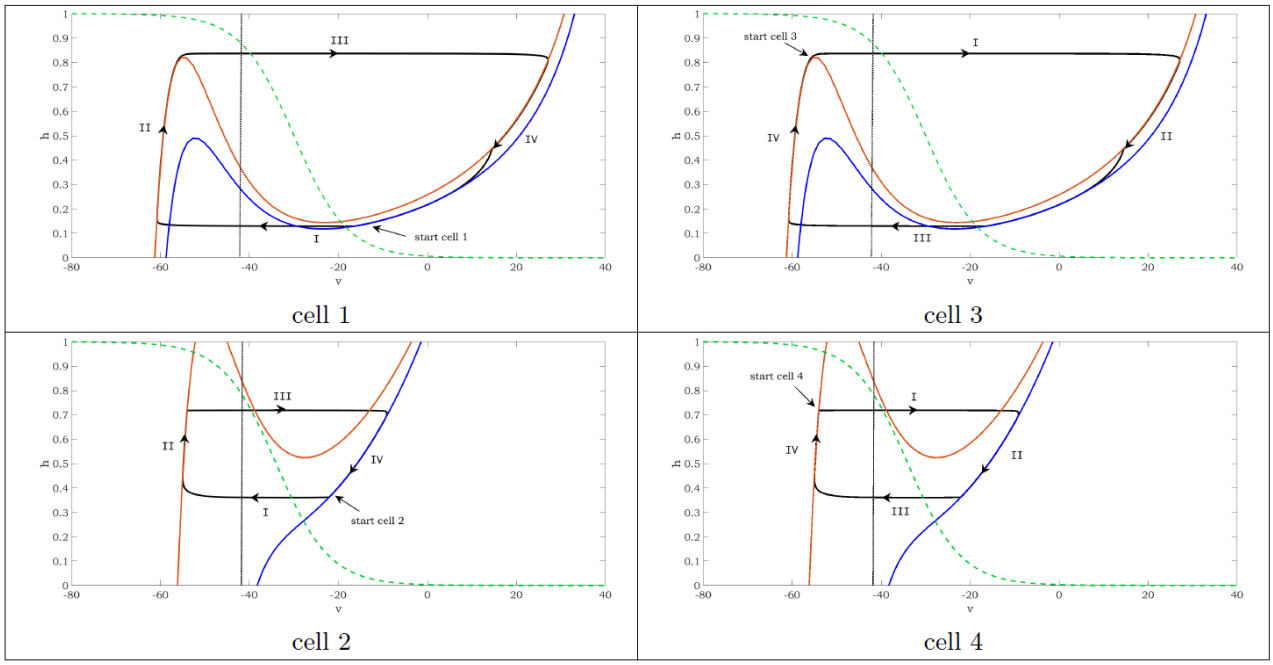

Figure 3: Basic nullcline configurations and periodic orbits for a four cell network with half-center oscillation mechanism in an excitatory escape regime. The solid lines are v-nullclines. The red cubic curves represents the inhibited v-nullclines while the blue curves represent the uninhibited v-nullcline for cells 1 and 3. For cells 2 and 4 the red cubic curves represents its unexcited v-nullclines while the blue curves represent their excited v-nullcline. The dashed green lines are slow variable nullclines, thick black lines are trajectories corresponding to half-center oscillation, and "vertical" dotted lines show synaptic threshold.

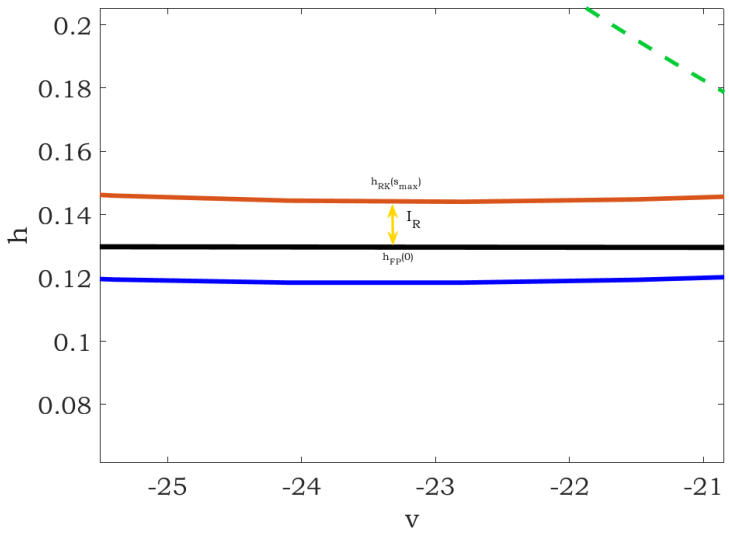

Figure 4: Zoomed in image of cell 1 shows the range of possible solutions for $I_R = [h_{fP}(0), h_{RK}(s_{max})]$ that will ensure cells 1 and 3 are able to jump to the silent phase in segment I.

3.1.2 Control of oscillation period and phase duration

Figure 2 shows us how periodic orbits behave for all four cells when all the cells are tuned to their *baseline drive*. Daun et al. [8] referred to this as a balanced case. Thus, we can now further study how changing the applied drives g_{app} can have an effect on the oscillatory responses through changes in the amplitude and ranges of the period of solutions for which oscillatory solutions continue to exist within the regime of the model.

3.1.2.1 Symmetric case The analysis of the symmetric case begins with setting the applied drive to cell 2 and cell 4 equal to each other to $g_{appI} = 0.1$ and the values of the applied drive of cell 1 and cell 3 are set equal to each other as well to $g_{appE} = 0.275$ as seen in Table 2. Note that these are the same values used for the phase plane analysis of the nullclines seen in Figure 3. For the excitatory escape regime, note that the dynamics of the system is driven by the excitatory cells 1 and 3. Therefore, these will be the paired cells for

which we will vary their g_{app_E} drive value, while maintaining g_{app_I}, the drive for paired cells 2 and 4, constant.

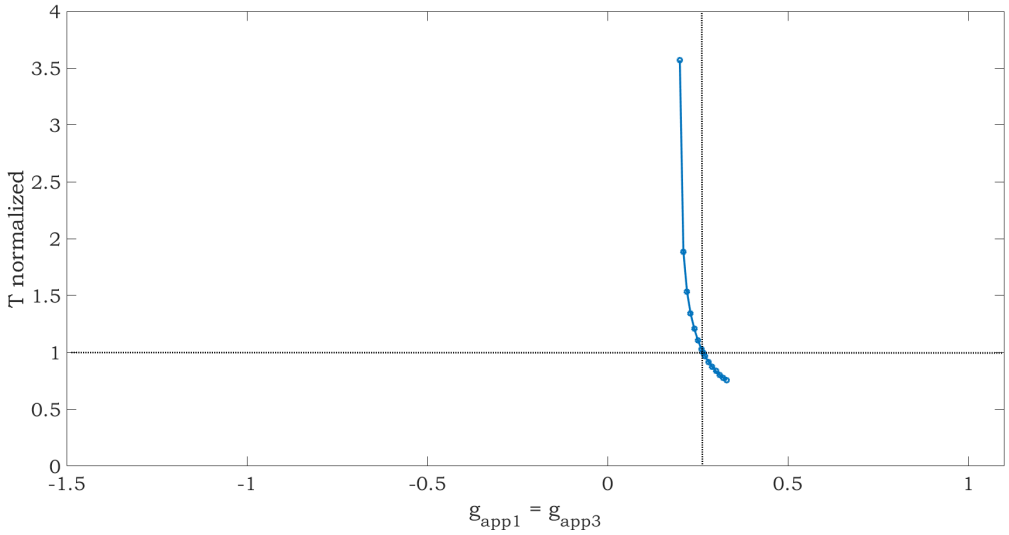

Figure 5: The periods of the basic periodic orbits shown in Figure 2 vary with changes in drive to both cells 1 and 3

As we vary g_{app_E}, we ensure that each periodic half-center solution persists, although the period will change. As we continue to change the drive by small uniform quantities, the periodic oscillations continue to change up to a maximum value of $g_{app_{E(max)}} = 0.35$ and a minimum value of $g_{app_{E(min)}} = 0.2$ for which the regime maintains the existence of periodic oscillations Figure 6. Thus we have a midpoint which we will denote as $g_{app_{E(0)}} = 0.275$, the same was done for the drives of cells 2 and 4 only to obtain its baseline drive which afterwards maintains itself constant for all further calculations. Note that at $g_{app_{E(min)}}$ we now are now approaching a fixed point at the left knee of the inhibited purple nullcline, thus the mechanism of the regime changes and the parameters prescribed for this method Table 2 no longer are able to support an oscillatory response.

The change of the period T of the oscillatory solution is the result of the different periodic ranges observed which vary under the influence of the different g_{app_E} values prescribed to the network. We will compare the changes in T in relation to the range of the the period at baseline drive $g_{\bar{app}}$, which we will denote as T_0. Therefore, the ratio of T/T_0 will allow us to normalize the solutions and compare the range of periods through the different periods

obtained by the variation of the g_{app_E} drive as illustrated in Figure 5.

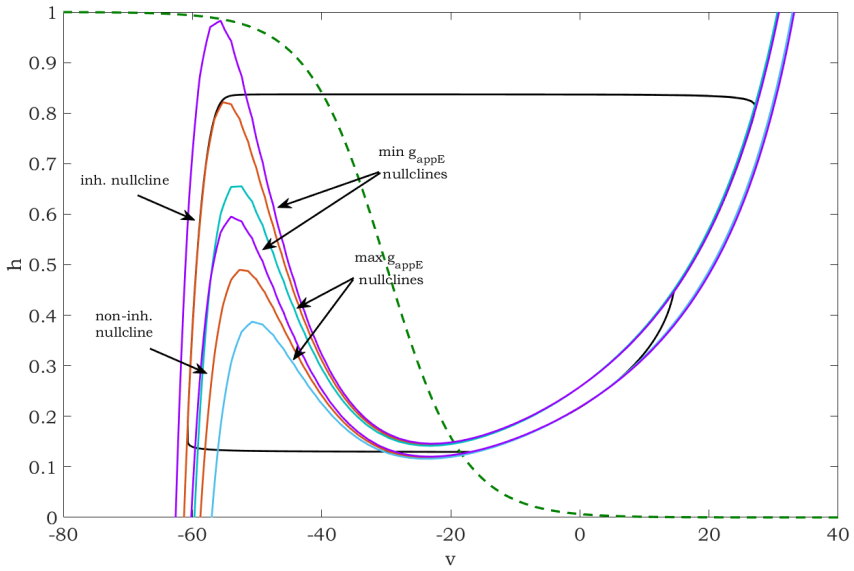

Figure 6: **Nullcline variation changes of g_{appE} of excitatory cells:** The red nullclines represents the inhibited and uninhibited v-nullcline at its baseline g_{appE} drive. The purple nullclines shows the shift of the v inhibited and uninhibited nullclines at $g_{appE(max)}$.The light blue nullclines shows the shift of the v inhibited and uninhibited nullclines at $g_{appE(min)}$

3.1.2.2 Asymmetric case Next, we considered the response of affecting the drive of only one cell for the excitatory escape half-center oscillation mechanism. We arbitrarily chose to give cell 1 the additional drive which will correspond to $g_{app_1} \neq g_{app_3}$, other than at its *baseline drive* which g_{app_3} is set to throughout. As in the *symmetric case*, we will consider all possible $|g_{app_1}|$ values for which we continue to have oscillatory solutions while maintaining the excitatory escape regime.

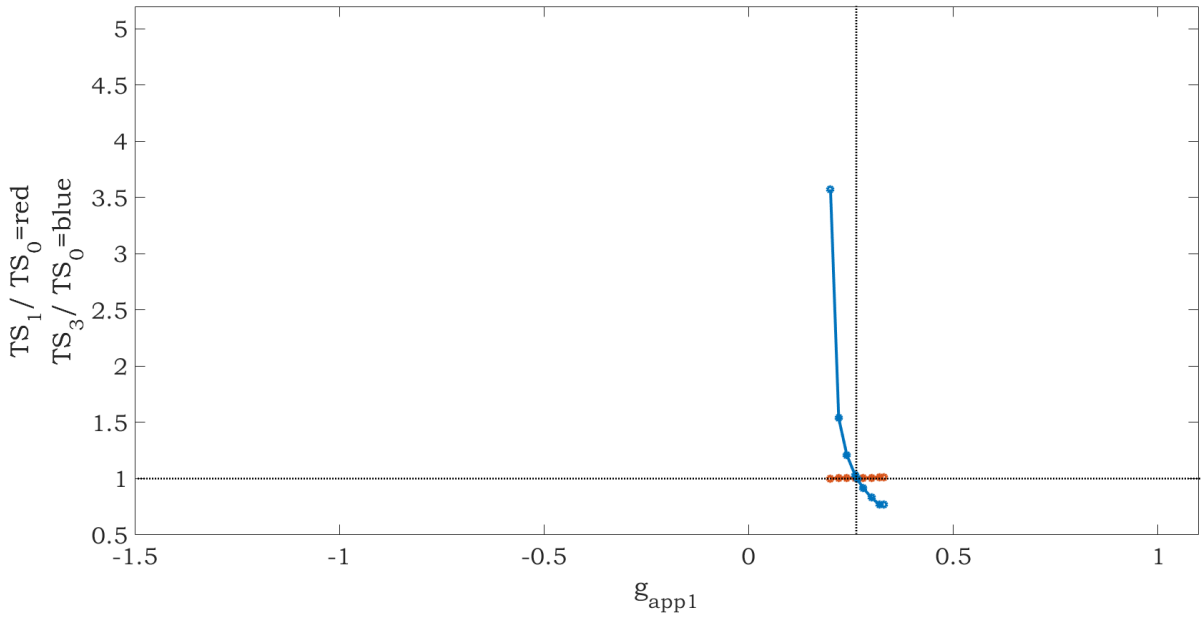

Figure 7: Changes in silent phase duration with changes in g_{app_1}, the drive to cell 1. In each plot, g_{app_3}, was held fixed at $\bar{g_{app}}$, the baseline drive for the corresponding model (*dotted vertical line*), and g_{app_1} was varied above and below that level. T_{s_1} and T_{s_3} denote the resulting silent phase durations of cells 1 and 3, respectively, and T_{s_0} (*dotted horizontal line*) denotes the silent phase duration with $g_{app_1} = g_{app_3} = \bar{g_{app}}$. Half-center oscillations based on persistent sodium current tuned to E-Escape

Figure 7 illustrates the changes in active phase duration that was numerically observed for a range of values of g_{app_1}. As we uniformly vary the values of the g_{app_1} similar to the *symmetric case*, we are able to find the relative range of g_{app_1} over which oscillatory behavior exists. We find that they are the same as we saw in Figure 5. It is clear that as we vary the values of g_{app_1}, the period changes of cell 1 are almost non existent. On the other hand, the period changes of cell 3 decrease drastically as g_{app_1} increases.

3.2 INHIBITORY ESCAPE MODEL

3.2.1 Half-center oscillation mechanisms

The parameters are now modified to fit the inhibitory regimes of where the inhibitory cells are driving the dynamics of the system within the escape model. Once again, each pair of inhibitory and excitatory cells are under the influence of different parametric values as described in Table 3. Moreover, this model is adjusted to allow the inhibitory cells 2 and 4 to drive the transition between the silent and active phases. Figure 9 presents the nullcline configuration of the baseline drive with the solution of its basic periodic orbit for each one of the four cells tuned now to an inhibitory escape regime. The oscillatory activity of the system is seen in Figure 8. In the absence of coupling cells 1 and 3 are tonically active while cells 2 and 4 are intrinsically excitable.

3.2.1.1 Parameters For the inhibitory escape model we list all parameter values necessary to maintain the desired regime with $\alpha = 1$:

Once again we can see that cells 1 and 2, and cells 3 and 4, are both active and silent almost precisely at the same time. Thus, all 4 cells are interacting and maintaining the inhibitory driven escape regime while maintaining continuous oscillatory solutions.

The nullclines seen in Figure 9 are structured similar to those seen in the *excitatory escape model*. The v-nullcline in blue is uninhibited while the red v-nullcline is inhibited for cells 1 and 3 while the v-nullcline in blue is excited while the red v-nullcline is unexcited for cells 2 and 4. The vertical dotted line, which shows the synaptic drive has now changed from this $\theta_{syn_E} = \theta_{syn_I} = -43$, previous case, to $\theta_{syn_E} = \theta_{syen_I} = -30$; this changes the position of the synaptic threshold. Also, note that with $\theta_{h_I} = -36$; the position of the h-nullcline is adjusted for the inhibitory cells. Also, the drive g_{NaP} effects for both inhibitory and excitatory cells has changed. In particular, g_{NaP_E} tripled in value which created changes in the v-nullcline. Note that while many of the parameters were tuned, we were still able to produce an escape regime driven by inhibitory cells.

The projection of the trajectory of cells 1 and 3 now lies close to the red inhibited nullcline

Excitatory cells	Values	Inhibitory cells	Values
g_{nap_E}	5.0	g_{nap_I}	5.0
g_{l_E}	1.6	g_{l_I}	1.6
g_{syn_E}	2	g_{syn_I}	3.4
$g_{app_{1,3}}$	0.45	$g_{app_{2,4}}$	0.185
θ_{m_E}	- 34.0	θ_{m_I}	-33.0
σ_{m_E}	-6.0	σ_{m_I}	-6.0
θ_{h_E}	- 30.0	θ_{h_I}	-36.0
σ_{h_E}	8.0	σ_{h_I}	6.0
θ_{syn_E}	- 30.0	θ_{syn_I}	-30.0
σ_{syn_E}	-0.2	σ_{syn_I}	-0.1

Table 3: We consider the set parameters necessary to maintain a regime of intrinsic escape.

in the silent phases and close to the blue noninhibited nullcline in the active phases. However, the trajectory of the solution is no longer passing through the right knee of the unihibited blue nullcline. Never-the-less, cells 2 and 4 have a projected trajectory that is close to the red unexcited nullcline in phase II and close to the blue excited nullcline during their active phases. Also, the trajectory of cells 2 and 4 now reach the left knee of the unexcited red nullcline.

Moreover, cell 3 and cell 4 are now in the active state of the trajectory as pointed by the arrows in Figure 9. Based on the dynamics of our network we know that cell 3, which is now in the uninhibited blue nullcline, excites cell 4 which is also in the blue excited nullcline. Cell 4 inhibits cell 1 which is now now in the red inhibited nullcline close to its knee as shown by the arrow. We will begin our phase cycle such that cell 3 and cell 4 are in the active state of the trajectory in phase I as pointed by the arrows labeled *start cell 3* and *start cell 4* in Figure 9 and this will be our starting point.

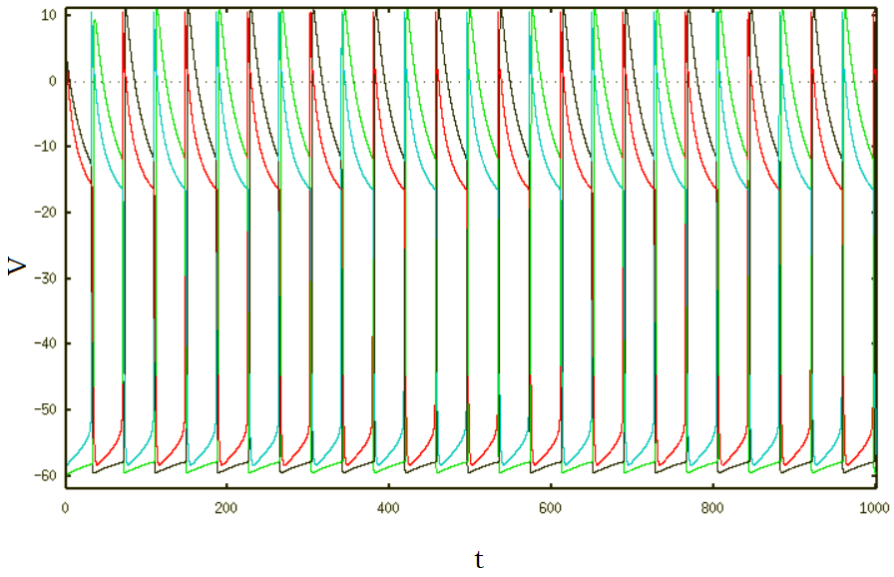

Figure 8: Time courses for periodic oscillations of cell 1 (black),cell 2 (red), cell 3 (green), cell 4 (blue) tuned to an inhibitory escape regime

Now, we see that cell 3 is exciting cell 4 which, in return, is inhibiting cell 1. As cell 2 has reached its top left knee of its unexcited nullcline and, since there is no fixed point at $v_{L_I}((h_1, 0)h_1)$, it is able to *escape* from its silent state and it starts moving along its trajectory in phase I. Although cell 2 is not escaping any inhibition, its escape arises when the silent cell reaches a point in phase space, namely the left knee of its red unexcited v-nullcline, and at this point it is able to jump to the active phase. Once it crosses its synaptic threshold it begins inhibiting cell 3 which now begins transitioning through its phase I. When cell 3 crosses its synaptic threshold, it stops exciting cell 4. As this happens, cell 4 crosses its synaptic threshold and starts to lose the inhibition it has on cell 1. Cell 1 therefore begins to move through its transition phase I eventually reaching its synaptic threshold. Once this happens, cell 1 begins exciting cell 2 which at this point is in phase II. Since cell 2 now receives excitation from cell 1 we see that it "jumps" from the unexcited nullcline to its excited blue nullcline.

Now, cell 2 is actively inhibiting cell 3 which now has to move to its inhibited nullcline.

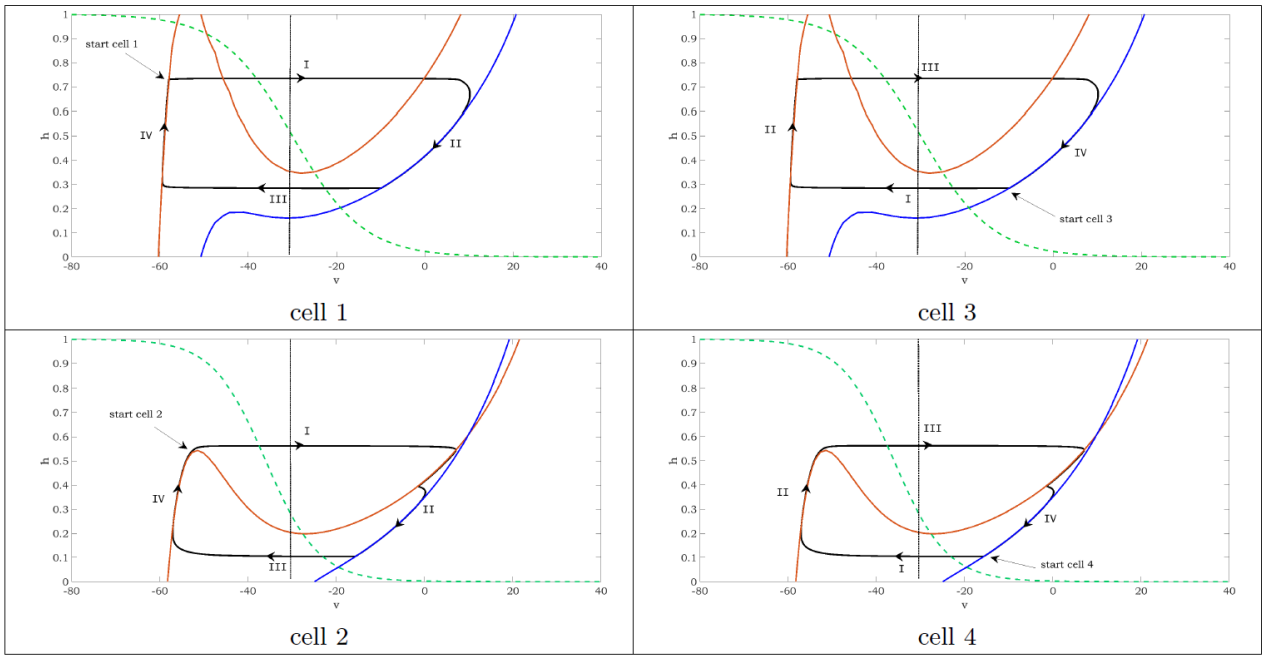

Figure 9: Basic nullcline configurations and periodic orbits for the four cell network with half-center oscillation mechanism for the inhibitory escape regime.The solid lines are v-nullclines. The red cubic curves represents the inhibited v-nullclines while the blue curves represent the uninhibited v-nullcline for cells 1 and 3. For cells 2 and 4 the red cubic curves represents its unexcited v-nullclines while the blue curves represent their excited v-nullcline. The dashed green lines are slow variable nullclines, thick black lines are trajectories corresponding to half-center oscillation, and "vertical" dotted lines show synaptic threshold

However, since it is below the knee of the red inhibited nullcline, it must jump to its hyperpolarized left branch. As it crosses its synaptic threshold, it halts excitation of cell 4 which must now also jump to its hyperpolarized left branch of the unexcited nullcline. Once it crosses its synaptic threshold it stops inhibiting cell 1 altogether. At this point, cell 1 is now in its uninhibited nullcline and active. Half an oscillatory cycle is performed and cell 1 is where cell 3 originally was, and similarly for cells 2 and 4. Repeating the same process with the new cell positions will finish the entire cycle and bring all cells back to their original positions.

Similar to the *excitatory escape regime*, we see that the trajectories of the inhibitory cells will transition from silent phase to the active phase from the left knee of the unexcited nullcline. Moreover, eventually they will descend through its silent phase toward a fixed point. The fixed point must remain above $h_{FP}(0)$. Hence, any h-values that are below $h_{FP}(0)$ will not be accessible to their trajectories. Also, note that all cells will jump down to the silent phase only if its trajectory is bellow the right knee of the red unexcited nullcline. This occurs only if $h_1 < h_{RK(S_{max})}$. Therefore, identical conditions for $I_R = [h_{fP}(0), h_{RK}(s_{max})]$ are necessary for this regime and, therefore, any $h_i \in I_R$ will ensures that the inhibited cell will depolarize above its synaptic threshold, terminating the activity of its pattern. Thus, the inhibited cell can escape from hyperpolarization; see Figure 4.

3.2.2 Control of oscillation period and phase duration

For the inhibitory escape regime we see that now the transitions of active and silent phases are driven by the inhibitory cells 2 and 4. The pair of inhibitory cells are under the drive of g_{app_I}. Due to the fact that these are the cells that initiate the dynamics, it is important to find how they influence the model within the mechanism of escape. We want to understand how changes in g_{app_I} will affect the frequency and range of the period while maintaining solutions of oscillatory responses within its regime (*inhibitory escape*).

3.2.2.1 Symmetric case Similar to the *excitatory escape regime*, we set the applied drive to cell 2 and cell 4 equal to each other at $g_{app_I} = 0.185$. The values of the applied drive to cell 1 and 3 are set to $g_{app_I} = 0.3$. For, this regime those values will be considered the *baseline drive*. As we vary the values of g_{app_I} through small uniform values, we will maintain the drives g_{app_E} of cell 1 and 3 constant. Periodic half-center solutions will persist for $0.07 \leq g_{app_I} \leq 0.3$, although the range of the period is changed. Thus, we have a midpoint $g_{app_I} = 0.185$.

The drive is changed by small uniform quantities, and the periodic oscillations continue to change along with their nullclines. In Figure 11, notice that at $g_{appI(min)}$ we now are approaching a fixed point at the left knee of the unexcited purple nullcline. As we slightly

decrease g_{appI} from $g_{appI(min)}$, we find that even when there is a release happening, the suppressed cell cannot jump to its active phase since the h value of the left knee of the excited nullcline is too close to the h value of the fixed point of its unexcited nullcline. Therefore, the trajectory cannot get large enough h in order to transition to its active state once it becomes released. At values greater than $g_{appI(max)}$, the active E cell gains a stable critical point in the active phase and thus can no longer release the suppressed cell. Thus, the mechanism of the regime changes and the parameters prescribed for this method Table 3 no longer are able to support an oscillatory response.

The period was normalized as described previously in *excitatory escape regime*. Thus, we are now able to compare the range of periods through the different periodic solutions obtained by variations of the g_{app_I} drive. Figure 10. However, contrary to the *excitatory escape regime*, we find that the range of periods are somewhat smaller.

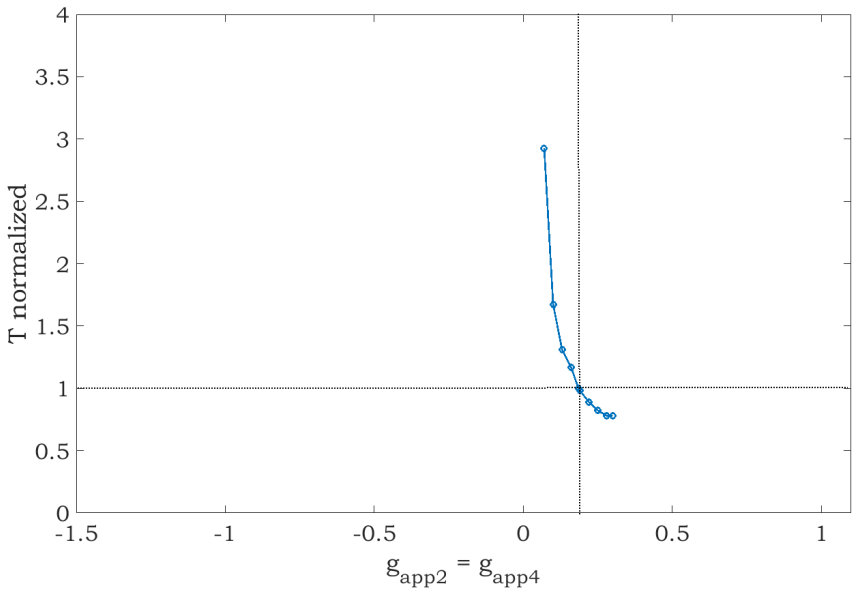

Figure 10: The periods of the basic periodic orbits shown in Figure 8 vary with the drive to both cells 2 and 4.

3.2.2.2 Asymmetric case Again, we see that the response of affecting the drive must be considered for only one the inhibitory cells. Due to the fact that the mechanism is now driven

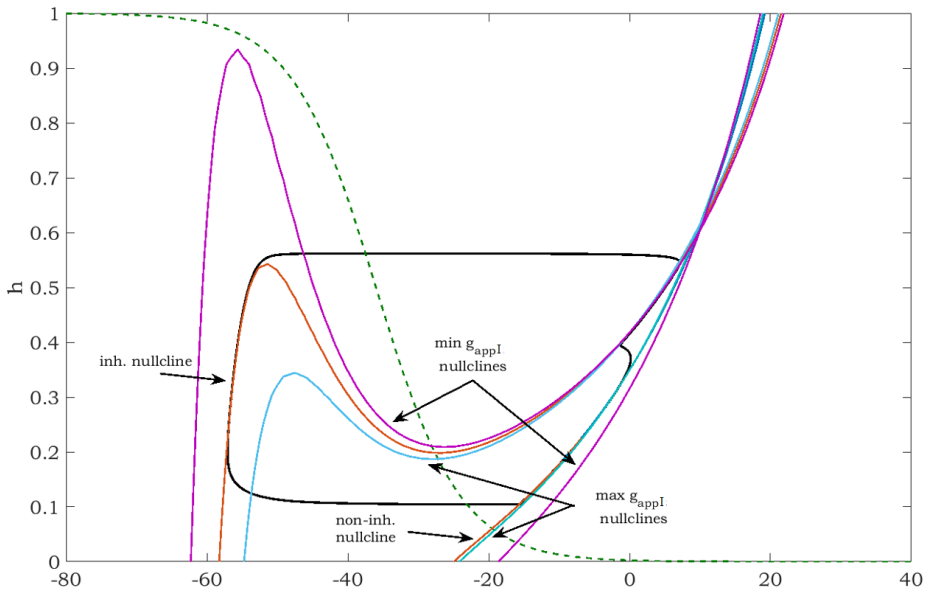

Figure 11: **Nullcline variation changes of g_{appI} of inhibitory cells:** The red nullclines represents the unexcited and excited v- nullclines set at its baseline g_{appI} drive. The purple nullclines shows the shift of the v unexcited and excited nullclines at $g_{appI(max)}$.The light blue nullclines shows the shift of the v unexcited and excited nullclines at $g_{appI(min)}$

by the inhibitory cells, we arbitrarily choose to give cell 2 the additional drive which will correspond to $g_{app_2} \neq g_{app_4}$, other than at its *baseline drive* which g_{app_4} is set to throughout. Also, for each half-center oscillation mechanism we consider that there is an existence of periodic oscillations while maintaining the *inhibitory escape regime*. It is clear that as the drive of cell 2 changes, the periods of cell 2 and cell 4 vary asymmetrically since the amplitude of the solutions in the trajectory of cell 2 maintains a normalized value. Simultaneously, cell 4 drastically decreases as the drive of cell 2 increases as seen in Figure 12.

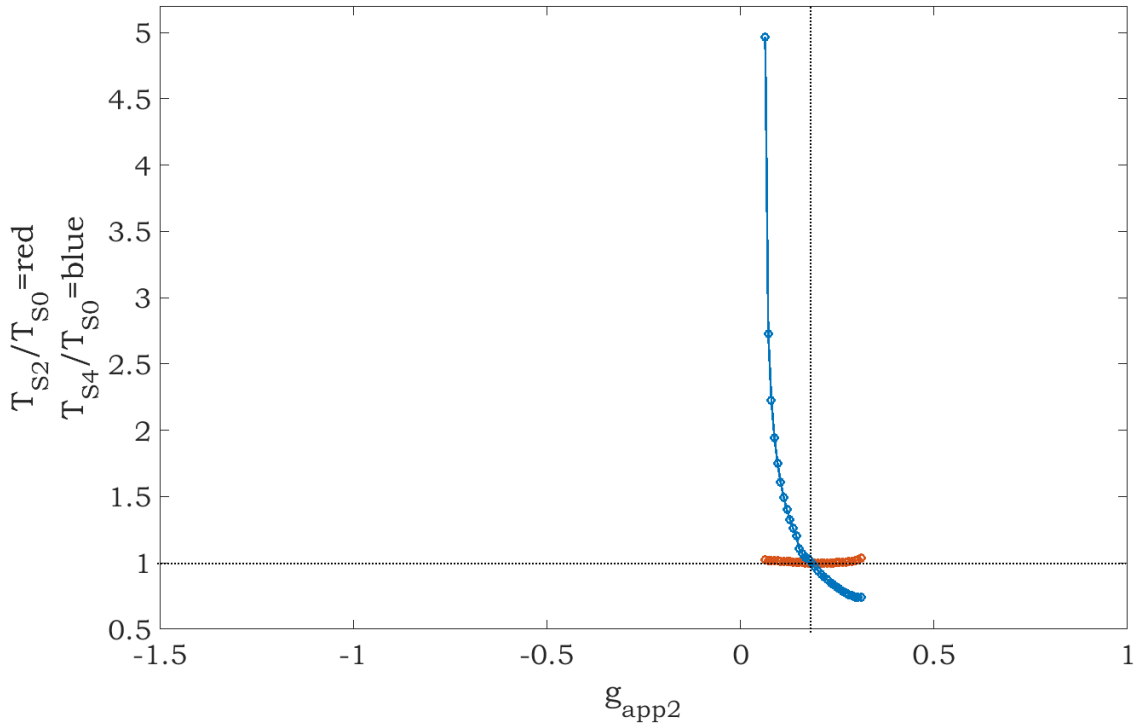

Figure 12: Changes in silent phase duration with changes in g_{app_2}, the drive to cell 2. In each plot, g_{app_4}, was held fixed at g_{app}^{-}, the baseline drive for the corresponding model (*dotted vertical line*), and g_{app_2} was varied above and below that level. T_{s_2} and T_{s_4} denote the resulting silent phase durations of cells 2 and 4, respectively, and T_{s_0} (*dotted horizontal line*) denotes the silent phase duration with $g_{app_2} = g_{app_4} = g_{app}^{-}$. Half-center oscillations based on persistent sodium current tuned to I-Escape

4.0 RELEASE MODEL

A *Release* mechanism is characterized to occur when a cell is active and its opposing cell is silent in a coupled network. The active cell is able to become silent when it starts losing excitation. Once it reaches the knee of its non-inhibitory/excited nullcline the active cell begins transitioning to a silent state and, as this cell crosses a particular threshold through its phase transition, its coupled silent cell can become active. This occurs not due to the silent cell escaping from inhibition of the active cell, but instead simply by being released from it. Note that if inhibition decays before its coupled cell can be released, this is no longer considered intrinsic release but rather release through adaptation; see **Chapter 5**.

4.1 EXCITATORY RELEASE MODEL

4.1.1 Half-center oscillation mechanisms

Again, the construction of periodic singular solutions are governed by the architecture seen in Figure 1. However, the model is now tuned to an excitatory release regime. Each pair of excitatory-inhibitory cells continue to be under the influence of synaptic inhibition. Due to the regime of this model, the dynamics are initiated by the excitatory cells. Moreover, for the release case, we know that oscillations must be primarily controlled by the cell in the active phase releasing the inhibited cell from its silent state. We can achieve this model under the following constraints.

4.1.1.1 Parameters For the excitatory release model, we list all parameter values necessary to maintain the regime. We set $\alpha = 3$ and:

Excitatory cells	Values	Inhibitory cells	Values
g_{nap_E}	5.0	g_{nap_I}	4.0
g_{l_E}	3.6	g_{l_I}	2.8
g_{syn_E}	1.5	g_{syn_I}	1.2
$g_{app_{1,3}}$	0.36	$g_{app_{2,4}}$	0.53
θ_{m_E}	- 34.0	θ_{m_I}	-31.0
σ_{m_E}	-8.0	σ_{m_I}	-6.5
θ_{h_E}	- 35.0	θ_{h_I}	-45.0
σ_{h_E}	8.0	σ_{h_I}	6.0
θ_{syn_E}	- 43.0	θ_{syn_I}	-43.0
σ_{syn_E}	-0.1	σ_{syn_I}	-0.1

Table 4: Parameters considered to maintain a regime of excitatory release model.

Based on the parameters set, we see that the maximal conductances of the sodium current in the excitatory cells was reduced by a third while the reversal potential of the synaptic current increased three times its value. However, the reversal potential for the applied current for both excitation and inhibitory cells increased to maintain the release regime.

As previously stated, we can see that cells 1 and 2 are both active or silent at almost precisely the same time, with cells 3 and 4 sharing this common trait as illustrated in Figure 13. While the excitatory release regime has oscillatory solutions, we see that the period of active and silent states are similar in frequency to the solutions seen in the *excitatory and inhibitory escape regimes.*

The phase plane of the nullclines is clearly illustrated in Figure 14 for all four cells. The vertical dotted line, which shows the synaptic threshold, has now changed to $\theta_{syn_E} = \theta_{syn_I} = -43$. Contrary to the excitatory escape model, we see that the g_{NaP} drive for the excitatory cell is reduced by a third while the synaptic drive g_{syn_E} of the excitatory cells

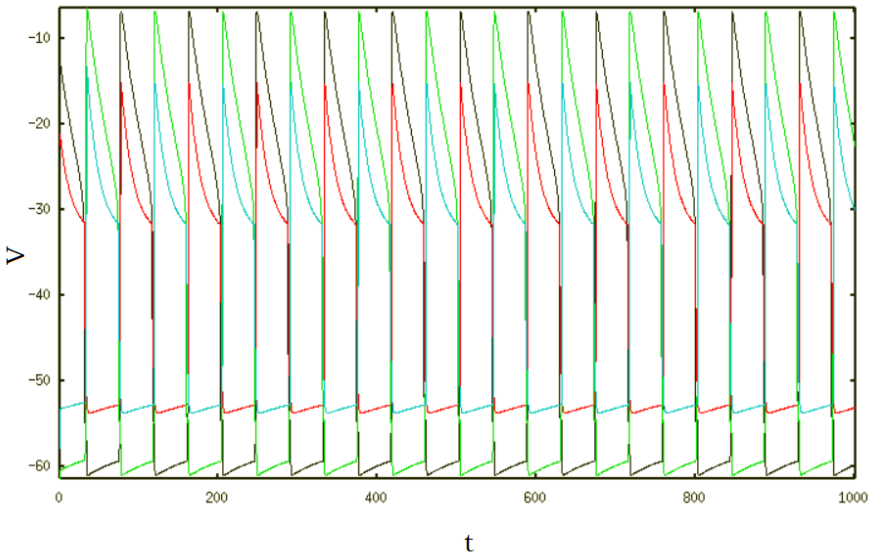

Figure 13: Time courses for periodic oscillations of four cells (cell 1 (black), cell 2 (red), cell 3 (green), cell 4 (blue)) tuned to an excitatory release.

tripled. Many other parameters have been slightly adjusted, however, we are still able to produce an excitatory regime now adjusted to a release mechanism.

The projection of the trajectory in cells 1 and 3 lie close to the blue uninhibited v-nullcline. The initial position of cell 1 and cell 2 are in the active phase in the blue uninhibited/excited v-nullcline, as pointed by the arrows labeled *start cell 1* and *start cell 2*.We will start here following the dynamics seen in Figure 1.

Given the dynamics of this model, we see that cell 1 is in the active phase and exciting cell 2 which in return is inhibiting cell 3. Cell 3 is currently in the red inhibited nullcline and in the silent phase as cell 4 is also silent and on its unexcited nullcline. However, cell 3 has a stable hyperpolarized equilibrium for the inhibition level it is receiving from cell 2. Therefore, cell 3 is currently contained in the silent state and since cell 1 does not have a stable active phase equilibrium, it moves along phase I. When this happens, cell 1 crosses its synaptic threshold denoted by the vertical dotted line. Thus cell 1 stops exciting cell 2 and cell 2 begins moving along its phase 1 until it reaches its synaptic threshold.

Once it crosses its synaptic threshold, cell 2 stops inhibiting cell 3 which is now *released* from inhibition and able to transition in its phase I and cross its synaptic threshold. Once cell 3 crosses its synaptic threshold, it begins exciting cell 4. When cell 4 becomes excited, it begins inhibiting cell 1. Cell 1 is not able to follow its trajectory due to the fast dynamics of the system. Consequently, the added inhibition, causes a jump to the hyperpolarized red v nullcline. In return, cell 1 stops exciting cell 2 which now transitions to its unexcited nullcline. Now, cell 1 and cell 3 have switched places from their original positions as have cells 2 and 4. This concludes half of an oscillatory cycle. Repeating the same process with new cell positions will bring them back to their original positions and completes the cycle.

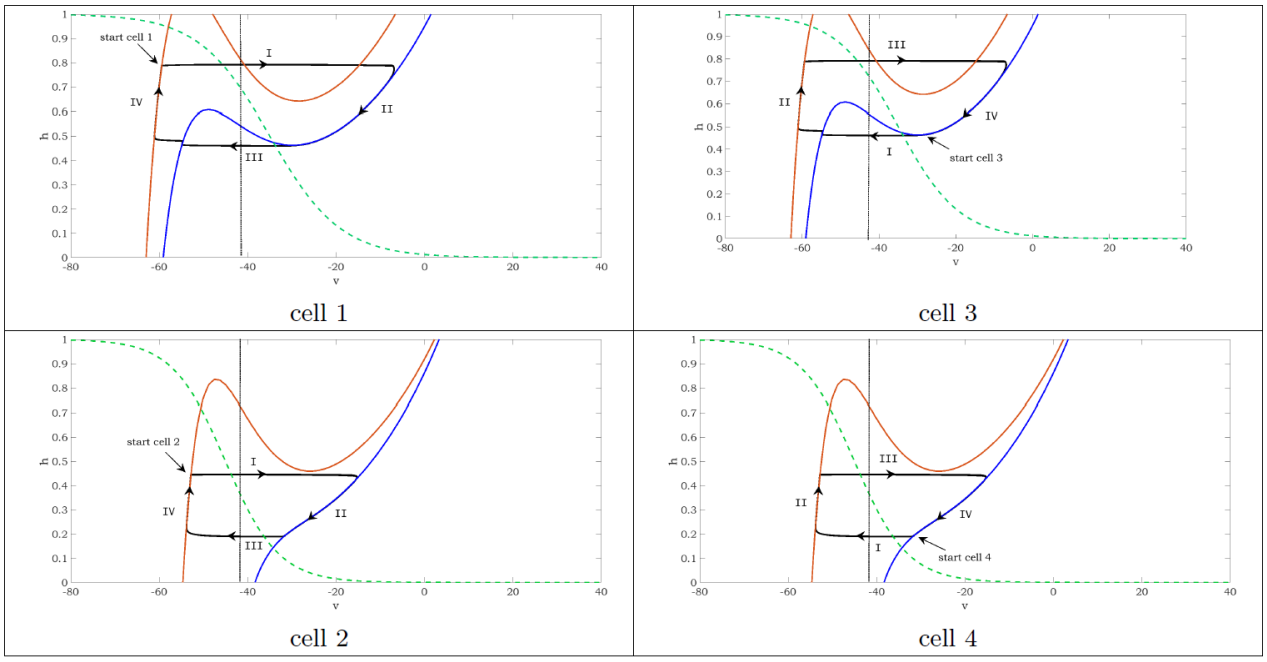

Figure 14: Basic nullcline configurations and periodic orbits for four cell connections with half-center oscillation mechanism for an excitatory release regime. The solid lines are v-nullclines. The red cubic curves represents the inhibited v-nullclines while the blue curves represent the uninhibited v-nullcline for cells 1 and 3. For cells 2 and 4 the red cubic curves represents its unexcited v-nullclines while the blue curves represent their excited v-nullcline. The dashed green line are slow variable nullclines, thick black line are trajectories corresponding to half-center oscillation, and dotted line shows synaptic threshold

Note that the trajectories of the cells 1 and 3 must jump to the silent phase as a result of the inhibition they received from their coupled cells that force a fast transition toward the silent phase. For cells 2 and 4 we see that their non-inhibited nullcline has a steep slope, and, while it allows for the existence of the oscillatory regime, we do not have a fixed point on the right knee. Let I_L, an interval analogous to I_R seen in the *escape mechanisms*, as $I_L \equiv [h_{LK}(0), h_{FP}(s_{max})]$ the interval between which a starting point given by $(v_L(h_2, s_{max}), h2)$ will maintain the regime provided that $h_2 \in I_L$, as illustrated in Figure 15. Same is true for cell 4.

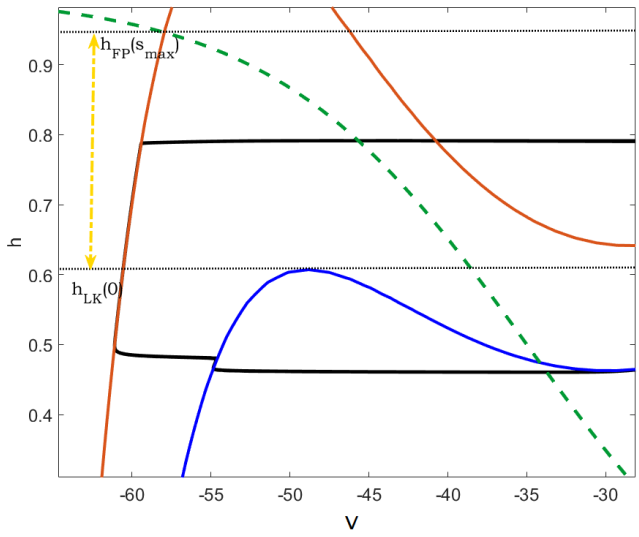

Figure 15: A zoomed image of cell 1 shows us the range of possible solutions for $I_L = [h_{fP}(0), h_{LK}(s_{max})]$ that will ensure cells 1 and 3 are able to jump to the active phase in segment IV.

4.1.2 Control of oscillation period and phase duration

4.1.2.1 Symmetric case For the excitatory release regime, we see that the dynamics of the *excitatory release mechanism* rely on the drive g_{appE} given to cells 1 and 3. Due to the fact that these are the cells that initiate the motion, we once again want to find how they influence the model. Moreover, we are interested in how the changes in parameters might

yield different possible solutions for the periodicity and amplitude of the solutions through different values of g_{appE}. We consider the changes of g_{appE} so long as the solution maintains oscillatory responses and stay within the *excitatory release regime.*

We will begin again by setting the baseline drive $g_{app_E} = 0.36$ and $g_{app_I} = 0.53$ for all four cells. Recall, these are the midpoint values for which the regime is able to maintain both oscillatory solutions and maintain it *excitatory release model.* Given that the excitatory cells instigate silent-active phase transitions of the regime, we will vary in drive g_{app_E} by small uniform quantities. The g_{app_E} values for which the periodic oscillations exist as we continue to change the applied drive are within a maximum of $g_{app_{E(max)}} = 0.65$ and a minimum of $g_{app_{E(min)}} = 0.07$. These bounds give us a midpoint of $\bar{g_{app_E}} = 0.36$ as illustrated in Figure 16.

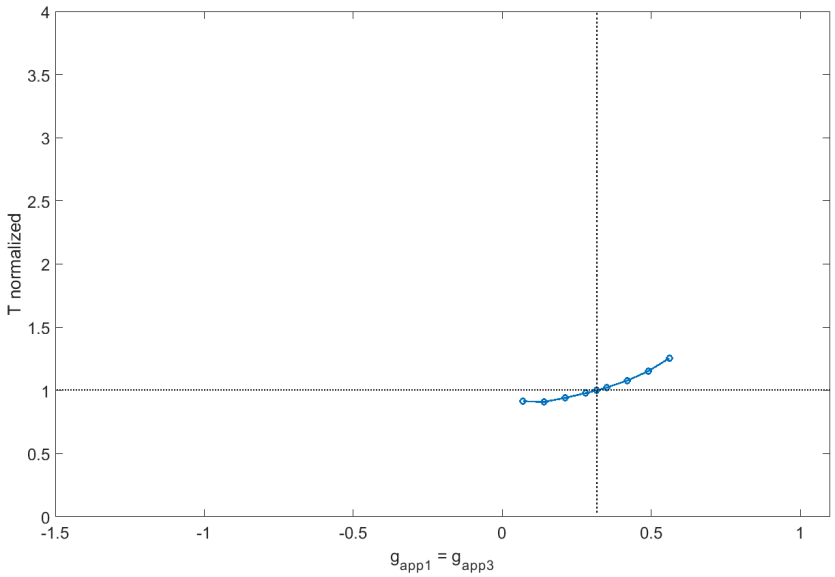

Figure 16: The periods of the basic periodic orbits shown in Figure 13 vary with changes in drive to both cells 1 and 3

Note that at $g_{appE(min)}$ we now are now approaching a fixed point at the left knee of the uninhibited purple nullcline. Also, we loose a fixed point on the left branch of the inhibited nullcline in the max values as shown by the light blue nullclines and instead get a fixed point on the middle branch of the inhibited nullcline. Thus, the mechanism of the regime changes

and the parameters prescribed for this method Table 4 no longer are able to support an oscillatory response beyond the range of g_{app_E} prescribed.

The period was normalized in the same manner as all previous cases and bearing this in mind we are able to compare the range of periods through the different periodic solutions obtained by the variations of the g_{app_E} drive. However, Figure 16 illustrates, we see that the period of the oscillations increase as the drive g_{app_E} is increased. This is contrary to what was found in the *excitatory regimes*.

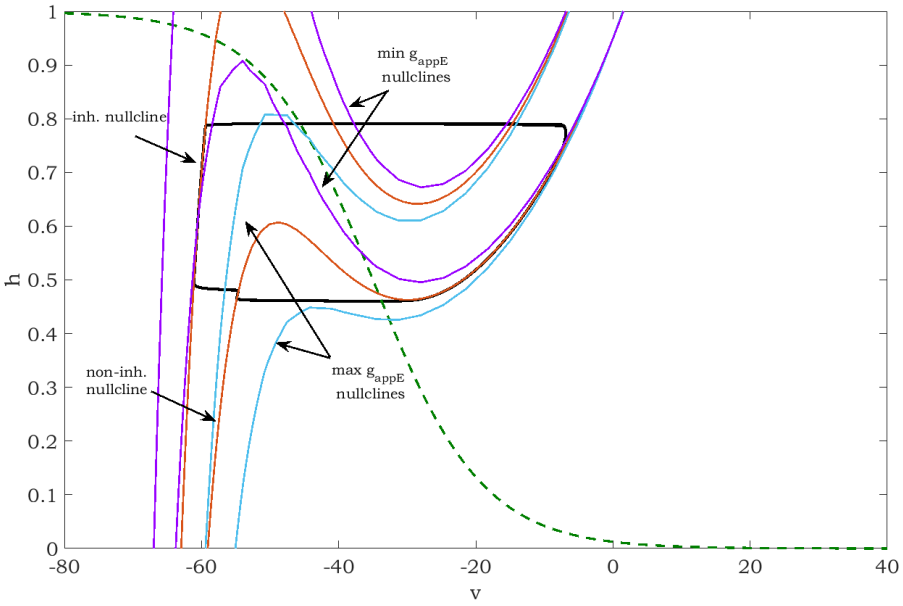

Figure 17: **Nullcline variation changes of g_{appE} of excitatory cells:** The red nullclines represents the inhibited and uninhibited v nullclines set at its baseline g_{appE} drive. The purple nullclines shows the shift of the v inhibited and uninhibited nullclines at $g_{appE(max)}$.The light blue nullclines shows the shift of the v inhibited and uninhibited nullclines at $g_{appE(min)}$

4.1.2.2 Asymmetric case Again, we want to consider responses of the oscillatory solutions affected by g_{app_E}. However, we know that we must arbitrarily choose only one of the excitatory cells to change drive while the applied drive of the other cells are maintained constant. We choose to change the values of drive g_{app_E} for cell 1 which will $g_{app_1} \neq g_{app_3}$.

This will be true always except at other the *baseline drive* for which g_{app_3} is set to this constant value throughout. For each half-center oscillation mechanisms, we consider that there is an existence of periodic oscillations while maintaining the *excitatory release regime*. It is clear that as the drive of cell 1 changes, it is now the period of *cell 3* that maintains itself relatively the same throughout. However, we find that as drive g_{app_1} increases, there is a direct change in the periods of *cell 1* which now also increase as their drive increases as seen in Figure 18.

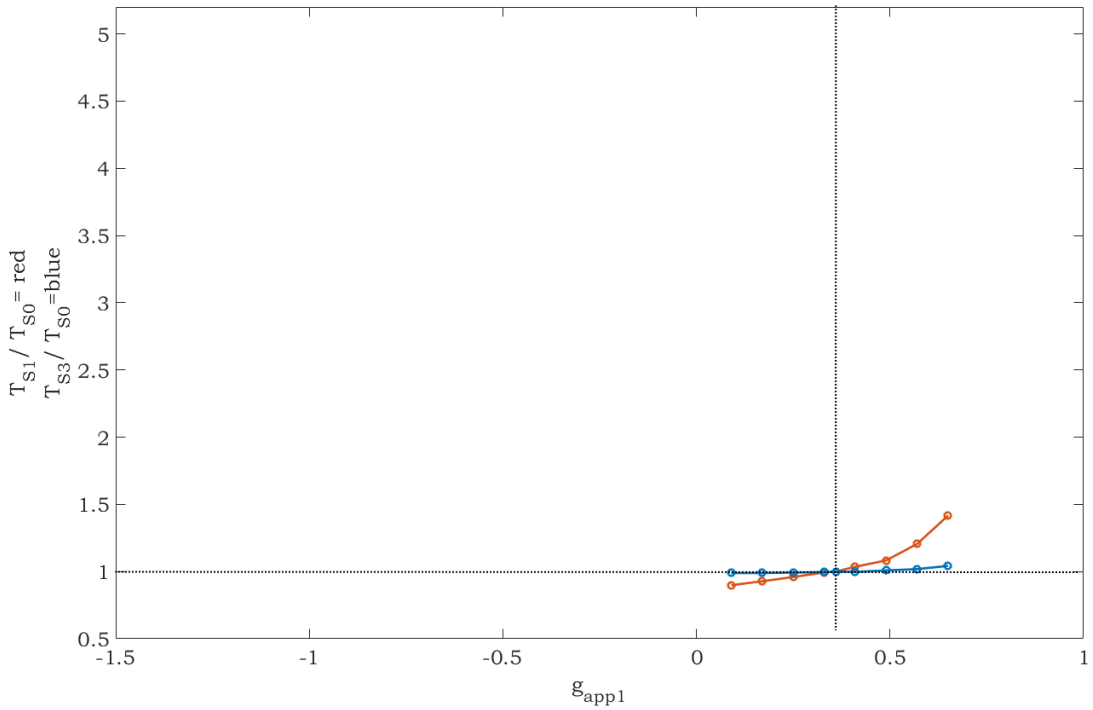

Figure 18: Changes in silent phase duration with changes in g_{app_1}, the drive to cell 1. In each plot, g_{app_3}, was held fixed at $\bar{g_{app}}$, the baseline drive for the corresponding model (*dotted vertical line*), and g_{app_1} was varied above and below that level. T_{s_1} and T_{s_3} denote the resulting silent phase durations of cells 1 and 3, respectively, and T_{s_0} (*dotted horizontal line*) denotes the silent phase duration with $g_{app_1} = g_{app_3} = \bar{g_{app}}$. Half-center oscillations based on persistent sodium current tuned to E-Release

4.2 INHIBITORY RELEASE MODEL

4.2.1 Half-center oscillation mechanisms

Similar to previous cases, the construction of periodic singular solutions are governed by the architecture seen in Figure 1. However, we must now consider a new set of parameters that will tune the model to an inhibitory release regime. Each pair of excitatory-inhibitory cells are the influence of synaptic inhibition. Moreover, the phase transitions of this model are initiated by the inhibitory cells. In particular for the release case, we know that the oscillations must be primarily controlled by the cell in the active phase releasing the inhibited cell from its silent state. We can achieve this model under the following constraints.

4.2.1.1 Parameters For the inhibitory escape model, we list all parameter values necessary to maintain the regime with $\alpha = 1$ and:

Excitatory cells	**Values**	**Inhibitory cells**	**Values**
g_{nap_E}	8.0	g_{nap_I}	5.0
g_{l_E}	2.6	g_{l_I}	2
g_{syn_E}	2	g_{syn_I}	0.75
$g_{app_{1,3}}$	0.32	$g_{app_{2,4}}$	-0.05
θ_{m_E}	- 34.0	θ_{m_I}	-34.0
σ_{m_E}	-6.0	σ_{m_I}	-6.0
θ_{h_E}	- 30.0	θ_{h_I}	-48.0
σ_{h_E}	8.0	σ_{h_I}	12.0
θ_{syn_E}	- 30.0	θ_{syn_I}	-35.0
σ_{syn_E}	-0.2	σ_{syn_I}	-0.1

Table 5: We consider the set parameters necessary to maintain a regime of intrinsic release model.

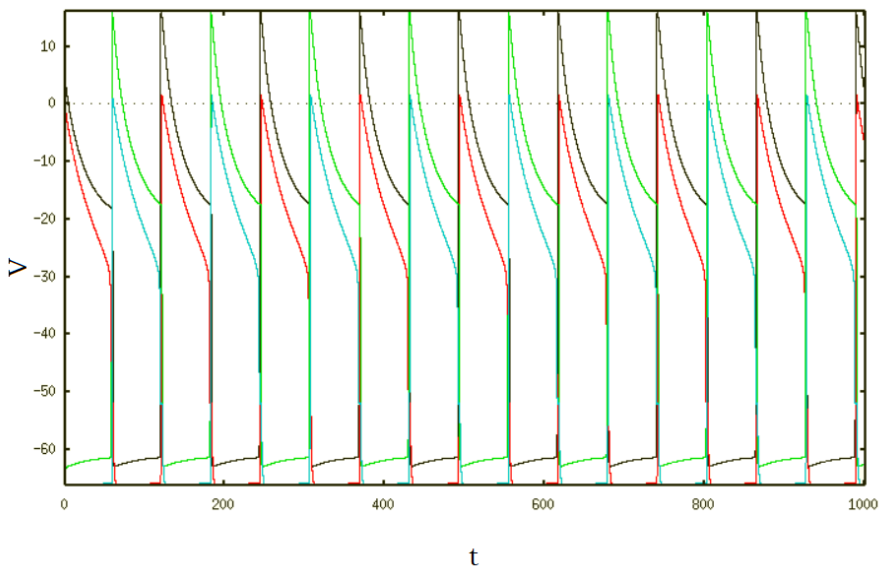

Figure 19: Time courses for periodic oscillations of four cells (cell 1 (black),cell 2 (red), cell 3 (green), cell 4 (blue)) tuned to an inhibitory release.

As previously stated, we can see that cells 1 and 2 are both active or silent at almost precisely the same time; cells 3 and 4 share this common trait as illustrated in Figure 19. While the inhibitory release regime has oscillatory solutions, we see that the period of active and silent states are very similar to those seen in the *excitatory release regime*.

Notice that the projection of the trajectory of cells 2 and 4 are now the ones close to the blue excited v-nullcline. The initial position of cell 3 is shown by the arrow in the blue uninhibited nullcline, as the position of cell 4 is on its excited nullcline. Due to the particular dynamics of our network, we see that cell 3 excites cell 4 which in return is inhibiting cell 1. Cell 1 on the other hand is currently positioned in the red inhibited nullcline as cell 2 is on its unexcited nullcline. Moreover, cell 1 has a stable hyperpolarized equilibrium fixed point, however, due to the inhibition level it receives from cell 4, it is contained in the silent state. Since cell 4 has reached the right knee of the excited nullcline, it starts transitioning through phase I. As cell 4 crosses its synaptic threshold it starts loosing the inhibition it has on cell 1 thus allowing it to begin its trajectory in phase I.

As cell 1 crosses its synaptic threshold, it begins exciting cell 2. Now, cell 2 is *released* and able to transition on phase I towards its excited nullcline. When it crosses its synaptic threshold, cell 2 begins inhibiting cell 3 which is now able to transition towards its inhibited nullcline. When it crosses its synaptic threshold it stops exciting cell 4 and that is why there is a jump in the trajectory of cell 4 through phase I from the excited to the unexcited nullcline. Now, cell 4 reaches its hyperpolarized nullcline and cells 1 and 2 become active as cells 3 and 4 are now silent. As all four cells continue their transitions through their phase II, cell 1 and cell 3 have switched places from their original positions as have cells 2 and 4. The entire cycle follows in the usual manner. In this regime find that the trajectories

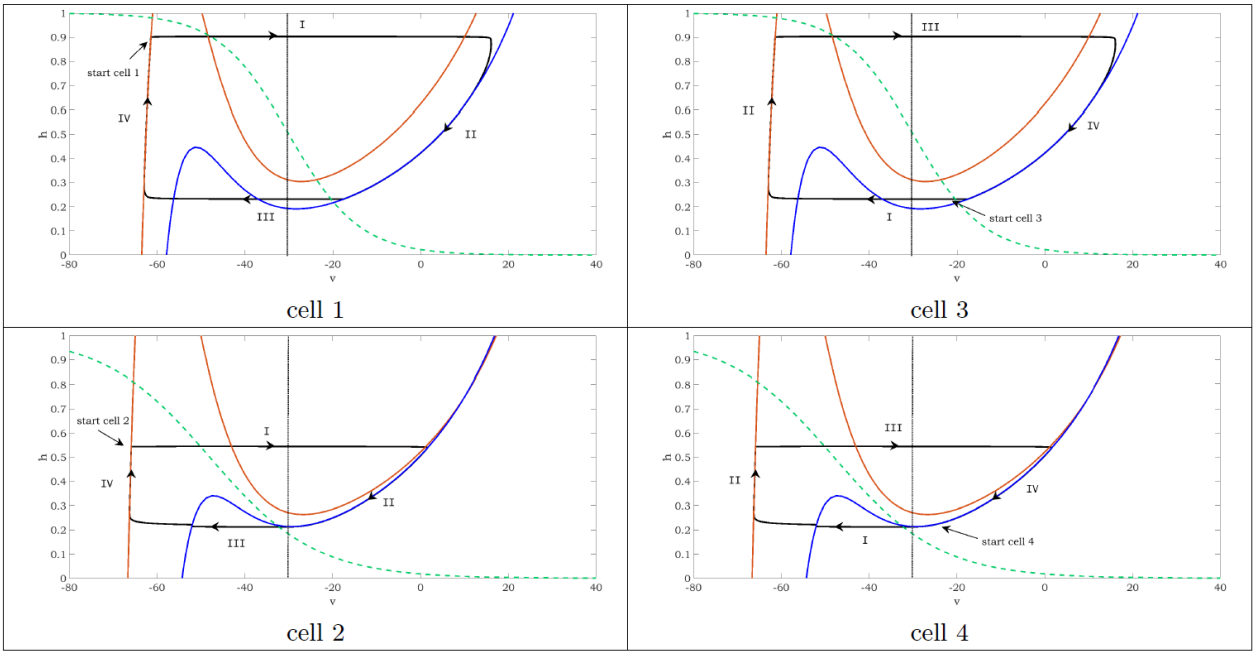

Figure 20: Basic nullcline configurations and periodic orbits for four cell connections with half-center oscillation mechanism tuned to an inhibitory release regime. The solid lines are v-nullclines. The red cubic curves represents the inhibited v-nullclines while the blue curves represent the uninhibited v-nullcline for cells 1 and 3. For cells 2 and 4 the red cubic curves represents its unexcited v-nullclines while the blue curves represent their excited v-nullcline. The dashed green line are slow variable nullclines, thick black line are trajectories corresponding to half-center oscillation, and dotted line shows synaptic threshold.

of cells 2 and 4 must jump to silent phase from the right knee of the excited active phase nullcline. They will descend through the excited nullcline toward a fixed point.However, cells 1 and 3 must be above the knee of its left uninhibited nullcline when it gets release in order to transition to its active phase. Thus, to reach the silent phase we must satisfy that if $h_E < h_{RK(S_{min})}$. Therefore, identical conditions for $I_R = [h_{RK}(s_{min}), h_{FP}(0)$ are necessary for this regime. Thus, for any $h_E \in I_R$ will ensures that the inhibited cell will depolarize above its synaptic threshold; see Figure 4.

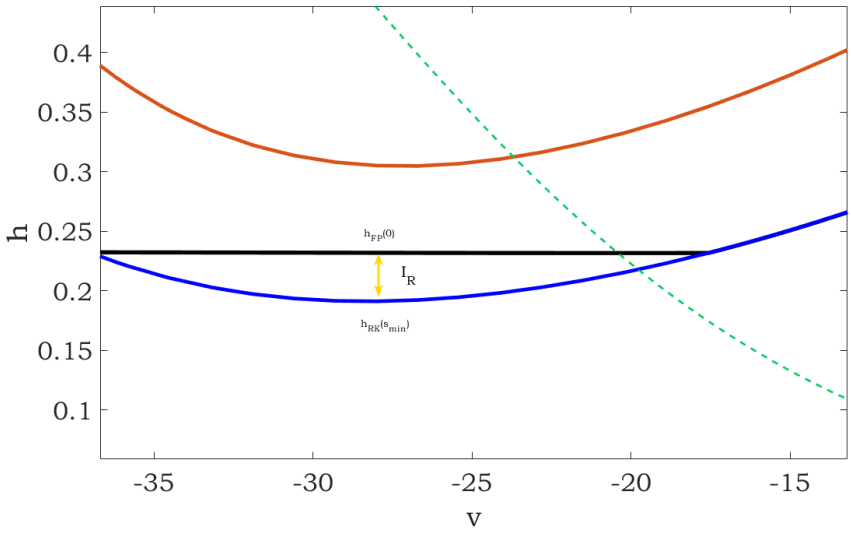

Figure 21: Zoomed in image of cell 1 shows the range of possible solutions for $I_R = [h_{RK}(s_{min}), h_{FP}(0)]$ that will ensure cells 1 and 3 are able to jump to the silent phase in segment I.

4.2.2 Control of oscillation period and phase duration

4.2.2.1 Symmetric case Given that the inhibitory release model relies on the drive of the *inhibitory* cells to initiate the dynamics of the system, we will study how changing the g_{appI} of cells 2 and 4 influences the periodic solutions of the model. We are interested in changes in amplitude and periodicity of responses while maintaining an oscillatory activity and staying within the regime of the method. Similar to previous cases, we consider the pair

of inhibitory cells under the drive g_{app_I} equal for 2 and 4 while fixed the drive and g_{app_E} for cells 1 and 3 constant.

The drive g_{app_I} is changed by small uniform quantities. The periodic oscillations continue to exist up to a lowest possible drive of $g_{app_I(min)} = -0.21$ and the largest possible values of $g_{app_I(max)} = 0.11$. The midpoint is therefore $g^{-}_{app_I} = -0.05$ which yields a negative *baseline drive*. Since this is an applied drive, we can consider this to be $|g_{app_I}|$, the negativity of the values does not necessarily mean that the behavior of the drive changes within the dynamics of the system. Once we fix $g^{-}_{app_I}$ we can find the period $\bar{T}$ that results from this drive. Note that at although the fixed points vary but stay in similar relation with the branches of the baseline drive, the parameters prescribed for this method Figure 23 no longer are able to support an oscillatory response after $g_{appI(max)}$ or before $g_{appI(min)}$.

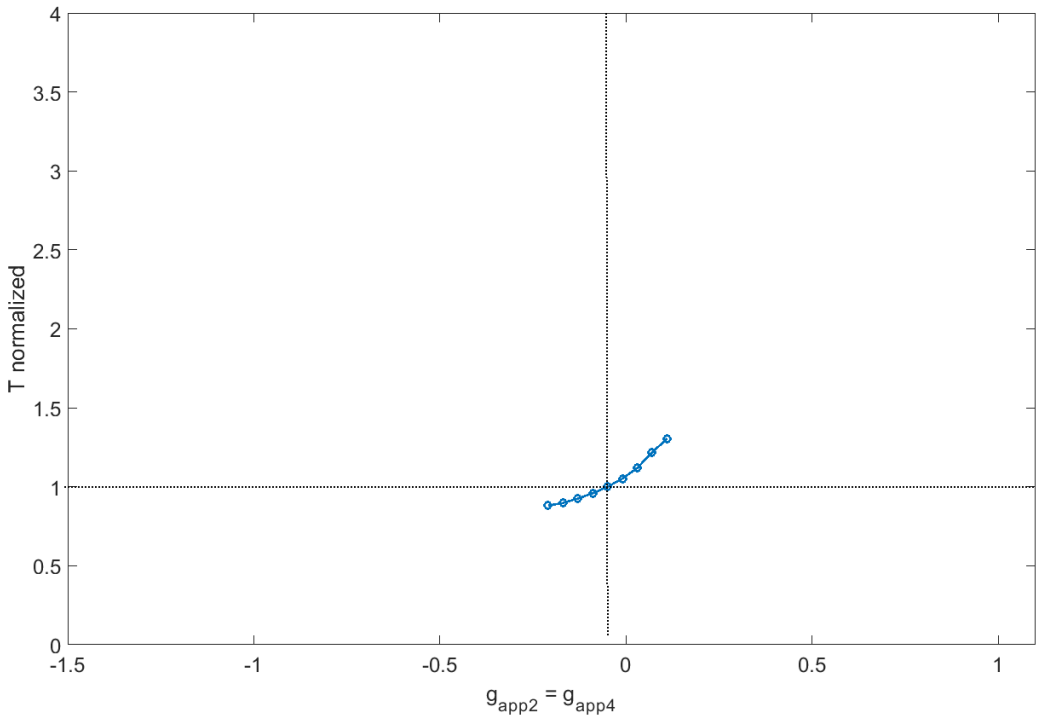

Figure 22: The periods of the basic periodic orbits shown in Figure 19 vary with changes to the drive of both cells 2 and 4

Moreover, the change of g_{app_I} in relation to the range of the total divided by g^{-}_{app} yields

the relative T of the system so that $\Delta T/\Delta g_{app_I}$ is the relative change of T compared to the relative range of g_{app_I} . Once again to, the *excitatory release model*, we see in Figure 22 that as g_{app_I} increases, the period of the oscillatory responses increase as well.

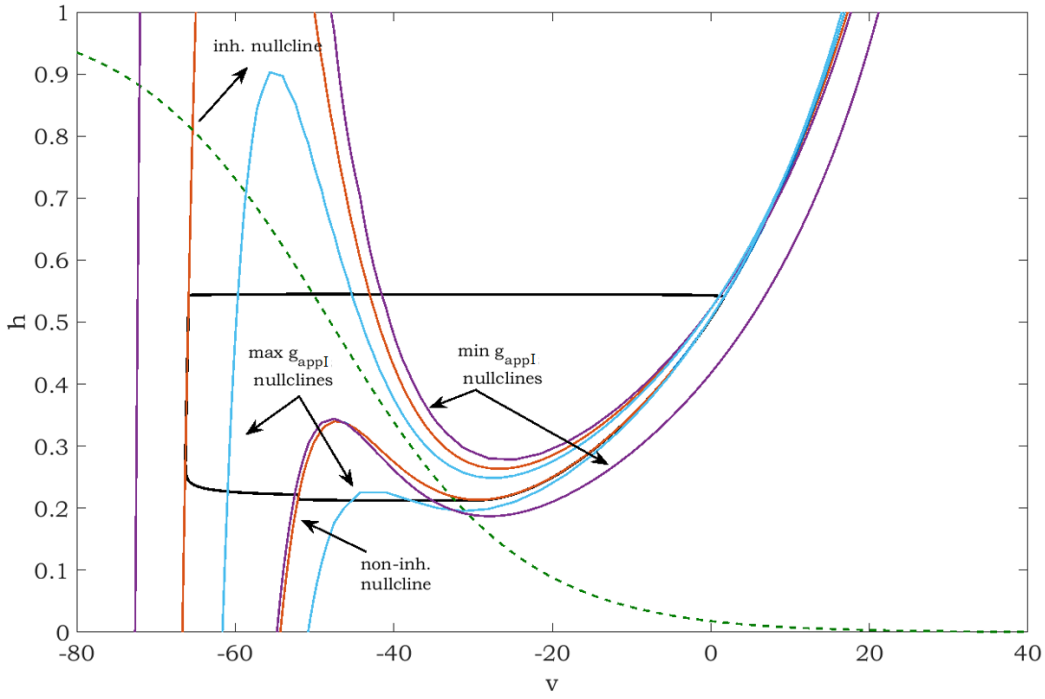

Figure 23: **Nullcline variation changes of g_{appI} of inhibitory cells:** The red nullclines represents the excited/unexcited v-nullclines set at their baseline g_{appI} drive. The purple nullclines shows the shift of the v excited/unexcited nullclines at $g_{appI(max)}$.The light blue nullclines shows the shift of the v excited/unexcited nullclines at $g_{appI(min)}$

4.2.2.2 Asymmetric case Now that we have found the response of the solution by affecting the drive g_{app_I} for both cells 2 and 4 paired together, we must now considered the effect of varying only one of the inhibitory cells. We arbitrarily choose to give cell 2 the additional drive which will correspond to $g_{app_2} \neq g_{app_4}$, other than at its *baseline drive* which g_{app_4} is set to throughout. Again, for each half-center oscillation mechanisms, we consider that are periodic oscillations and find sufficient conditions for which we continue to see the existence of the oscillatory solution while maintaining the *inhibitory release regime*.

In Figure 24, we find that the relative range of possible solutions is very small, as we saw in the *excitatory release regime*, and follows a similar trend. The drive of g_{app_2} is increased, the period of the response of cell 2 increases as well while cell 4 maintains itself with similar oscillatory responses throughout all value changes of g_{app_2}.

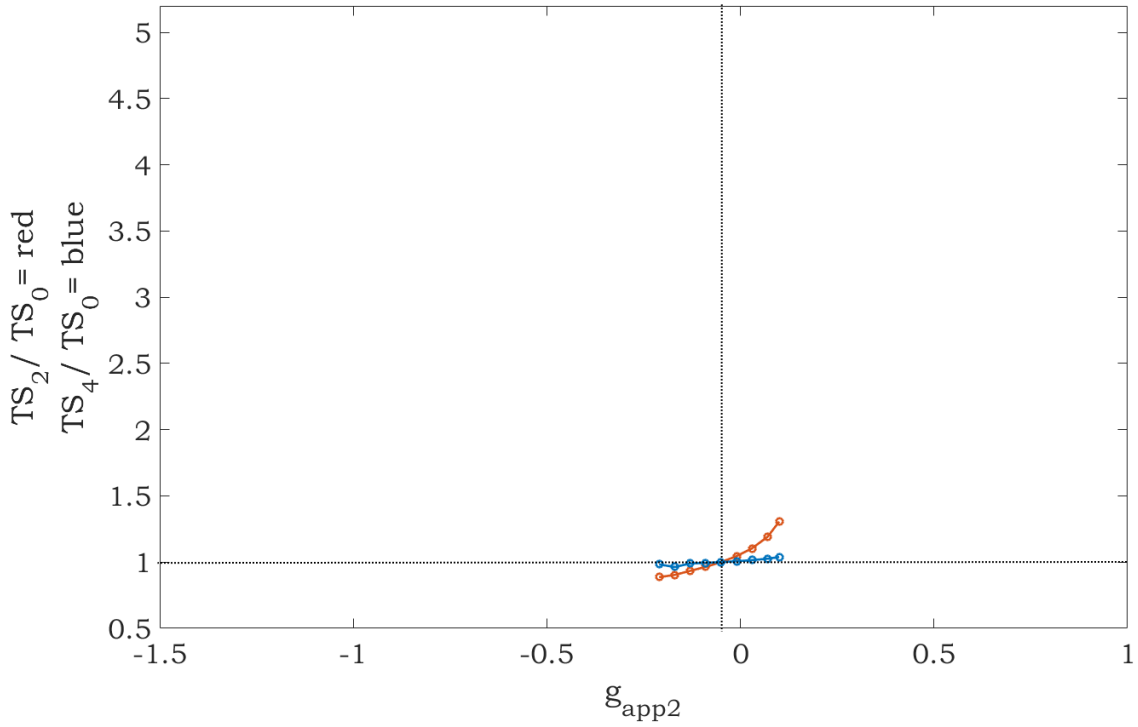

Figure 24: Changes in silent phase duration with changes in g_{app_2}, the drive to cell 2. In each plot, g_{app_4}, was held fixed at g_{app_0}, the baseline drive for the corresponding model (*dotted vertical line*), and g_{app_2} was varied above and below that level. T_{s_2} and T_{s_4} denote the resulting silent phase durations of cells 2 and 4, respectively, and T_{s_0} (*dotted horizontal line*) denotes the silent phase duration with $g_{app_2} = g_{app_4} = \bar{g_{app}}$. Half-center oscillations based on persistent sodium current tuned to I-Release

5.0 ADAPT ESCAPE AND RELEASE MODELS

Different studies have explored various models and their transitions in which an active cell or unit becomes silent and a silent cell or unit becomes active through mechanisms of escape and release. However, it has been noted that in some cases, the transitions between silent and active phases could happen due to partial release or adaptation of a cell [30, 33, 8]. It was noted that when one neuron was intrinsically bursting it was able to jump for a silent to an active phase or vice-versa on its own, in the absence of inhibition. Yet, in a coupled network there may be the possibility that when one of the cells is active and the other one is silent, if the silent cell is below a given synaptic threshold it is not able to inhibit the active cell and therefore cannot become active.

Never-the-less, it was observed that there is a way to *adapt* the responses by moving the synaptic threshold out of the interval range between the "upjump" and "downjump" voltages of the coupled system as, described by Skinner et al. [30]. The "*upjump* voltage" is the voltage value when the cell transitions from silent to active. The "*downjump* voltage" is the voltage value when the cell transitions for active to silent, as seen in the phase planes of the h and v nullclines. Thus, the synaptic threshold can be shifted to an interval of voltages through the uninhibited and inhibited v-nullclines which will mark the difference between *adapt escape* and *adapt release* regimes.

5.1 ADAPT INHIBITORY ESCAPE MODEL

5.1.1 Half-center oscillation mechanisms

The basic architecture is illustrated in Figure 1. However, we must ocne again adjust to our new regime and fine tune the parameters to allow the inhibitory cells 2 and 4 to drive the transition between the silent and active phases while instigating the same transitions for cells 1 and 3. Therefore, we must now consider the added element of the synaptic drive and it interaction with the phase transitions of the trajectories of cell solutions.

5.1.1.1 Parameters Again, for the adapt escape inhibitory method, we list all parameter values necessary to maintain the regime. Letting $\alpha = 1$ and:

Excitatory cells	Values	Inhibitory cells	Values
g_{nap_E}	7.0	g_{nap_I}	5.0
g_{l_E}	2.0	g_{l_I}	4.0
g_{syn_E}	1	g_{syn_I}	3
$g_{app_{1,3}}$	0.495	$g_{app_{2,4}}$	- 0.33
θ_{m_E}	- 31.0	θ_{m_I}	-34.0
σ_{m_E}	-5.0	σ_{m_I}	-6.0
θ_{h_E}	- 47.0	θ_{h_I}	-34.0
σ_{h_E}	8.0	σ_{h_I}	8.0
θ_{syn_E}	- 30.0	θ_{syn_I}	-10.0
σ_{syn_E}	-4.0	σ_{syn_I}	-4.0

Table 6: We consider the parameter set necessary to maintain a regime of inhibitory adapt escape model

In Figure 26, the trajectories of the solutions seen are almost identical to those seen in both escape regimes in **Chapter 3**. However, the main changing feature that allows for this

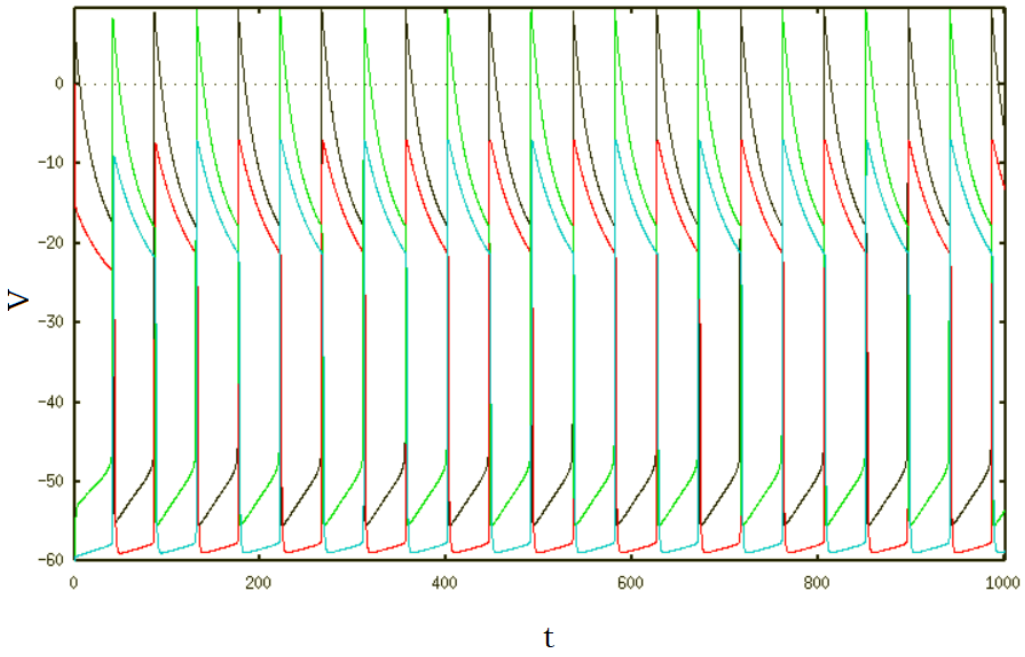

Figure 25: Time courses for periodic oscillations of four cells (cell 1 (black),cell 2 (red), cell 3 (green), cell 4 (blue)) set to an inhibitory adapt escape regime.

oscillatory response is the synaptic threshold (as indicated by the dotted lines in Figure 26) that is particularly shifted for the "inhibitory cells", while the synaptic threshold of the excitatory cells is still within the trajectory in phase I. Evidently, we now have different threshold for $\theta_{syn_E} = -30$ and $\theta_{syn_I} = -10$.

Given the adjustment of the dynamics of this model, we see that cell 3 lies in the excited blue v-nullcline at the beginning of the active phase I, as cell 4 is also active in its excited nullcline. Cells 1 and 2 are in their silent state.

As cell 4 has passed its synaptic threshold in phase IV, it no longer is actively inhibiting cell1. Therefore, cell 1 is able to transition through its phase I towards its uninhibited nullcline. When cell 1 crosses its synaptic threshold, the voltage is large enough to excite cell 2 and reach its active phase. Therefore, cell 2 now starts its transition through phase I and is able to *escape* its silent state. As it crosses its synaptic threshold it begins inhibiting cell 3, which is no longer able to excite cell 4 as it crosses its synaptic threshold, reaches

its inhibited nullcline. Cell 4 at this point is also silent and on its unexcited nullcline. At this point, we have completed half a cycle where cell 1 and cell 3 have switched initial positions, as have cells 2 and 4. The full cycle is completed in the usual way. Note, that same requirements of the trajectory are true for cells 1 and 3 as those seen in the intrinsic escape case described in Figure 4.

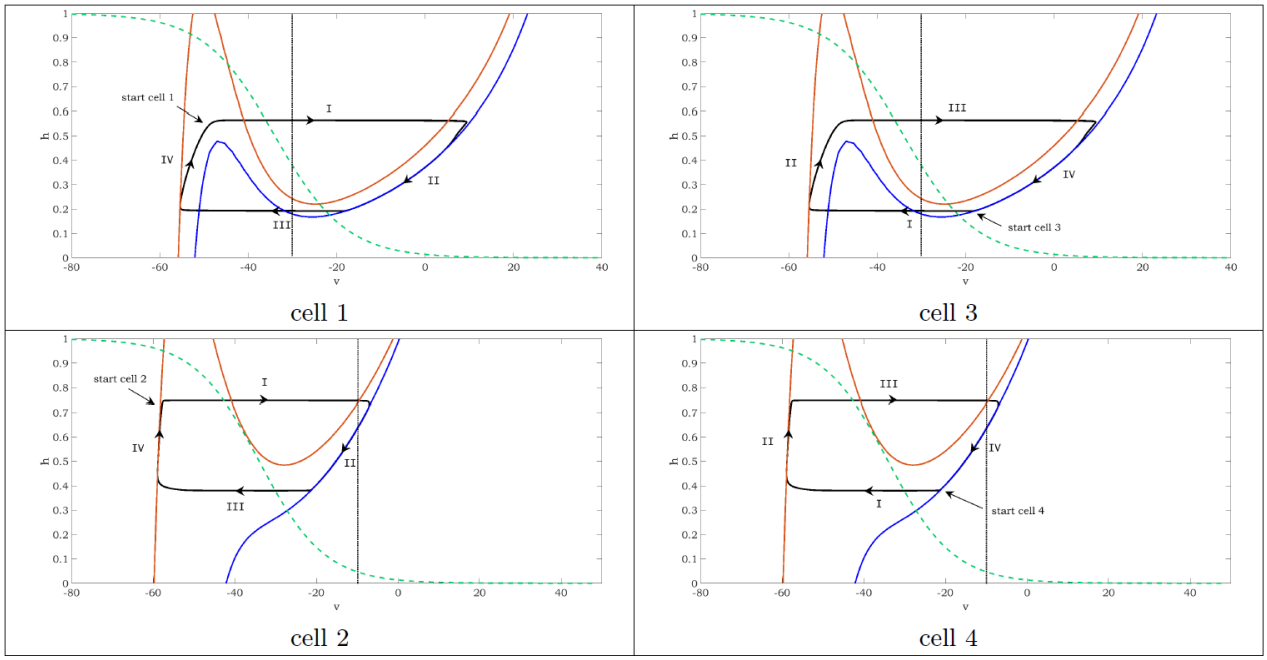

Figure 26: Basic nullcline configurations and periodic orbits for four cell connections with half-center oscillation mechanism tuned to an inhibitory adapt escape regime. The solid lines are v-nullclines. The red cubic curves represents the inhibited v-nullclines while the blue curves represent the uninhibited v-nullcline for cells 1 and 3. For cells 2 and 4 the red cubic curves represents its unexcited v-nullclines while the blue curves represent their excited v-nullcline. The dashed green line are slow variable nullclines, thick black line are trajectories corresponding to half-center oscillation, and dotted line shows synaptic threshold.

5.1.2 Control of oscillation period and phase duration.

5.1.2.1 Symmetric case Since our model regime is tuned to the adapt *inhibitory* escape model, it relies on the drive of the *inhibitory* cells to initiate the dynamics of the system.

Therefore, we now consider how changes in the drive g_{appI} of cells 2 and 4 may influence the periodic solutions of the model, considering any effect that the synaptic current may have on the results. Changes begin again by considering cells 2 and 4 to be under the influence of the same drive g_{app_I}, while also maintaining cells 1 and 3 under the same constant drive g_{app_E}, as seen in Table 6.

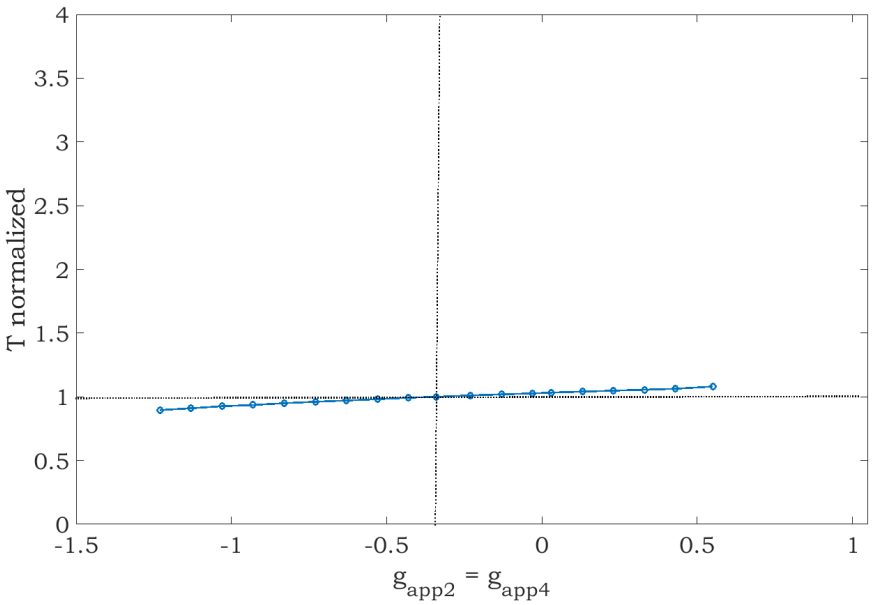

Figure 27: The periods of the basic periodic orbits shown in Figure 25 vary with changes in drive to both cells 2 and 4

The drive g_{appI} for cells 2 and 4 is varied through small uniform quantities over a range of possible values for which oscillatory solutions exists, while staying within its regime. The lowest possible drive prescribed is $g_{appI(min)} = -1.23$ and the maximum value is $g_{appI(max)} = 0.55$. This gives us a midpoint at $g^{-}_{appI} = -0.33$. Note that the nullclines of the varied drive g_{appI} and change the position of the fixed points. However, these fixed points stay in similar relation within the left branches of the unexcited nullcline as when baseline drive g^{-}_{appI} is prescribed. At values greater than $g_{appI(max)}$ it is possible that the mechanism is now able to escape on its own without the input of the synaptic threshold. At values smaller than $g_{appI(min)}$ it is possible that the synaptic threshold is no longer strong enough to allow for an escape mechanism. If g_{appI} is varied outside of the range of possible values, the parameters

for this method Figure 28 no longer are able to support an oscillatory response.

The change of g_{app_I} in relation to the range of the total divided by $\bar{g_{app}}$ gives us the relative range of the period T which is normalized with the period $\bar{T}$ obtained from using the baseline drive $\bar{g_{app_I}}$. Now, we find that $\Delta T/\Delta g_{app_I}$ is the relative change of T compared to the relative range of g_{app_I}. Moreover, we find that the range of oscillatory solutions for this regime is significantly larger than any other model. While the amplitude of the solutions of the active phase is not very large, we find a longer maintenance of solution existence in this regime compared with any other method.

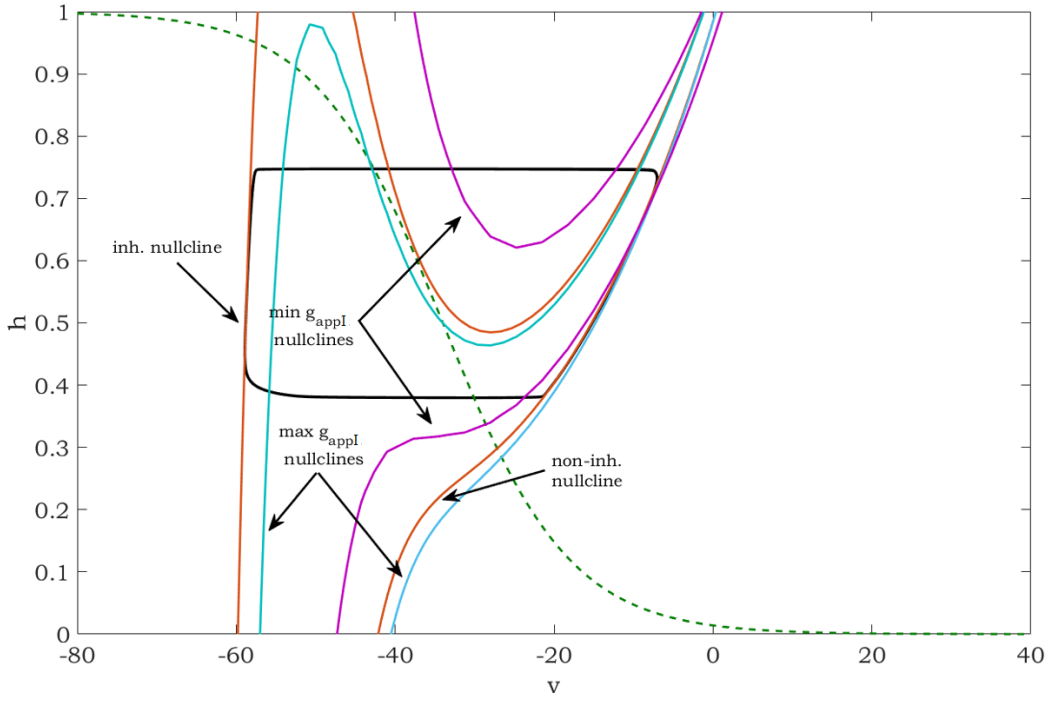

Figure 28: **Nullcline variation changes of g_{appI} of inhibitory cells:** The red nullclines represents the excited/unexcited v-nullclines set at its baseline g_{appI} drive. The purple nullclines shows the shift of the v excited/unexcited nullclines at $g_{appI(max)}$.The light blue nullclines shows the shift of the v excited/unexcited nullclines at $g_{appI(min)}$

5.1.2.2 Asymmetric case It is of interest to find the response of changes in drive for only one of the inhibitory cells. Cell 2 is chosen to receive the additional drive which will

correspond to $g_{app_2} \neq g_{app_4}$, other than at its *baseline drive* which g_{app_4} is set to throughout. Similar to the results seen in the inhibitory escape case, the period of cell 2 maintains itself nearly constant throughout uniform increases to g_{app_2}. However, we see the period of cell 4 increases slightly as g_{app_2} increases throughout, as illustrated in Figure 29.

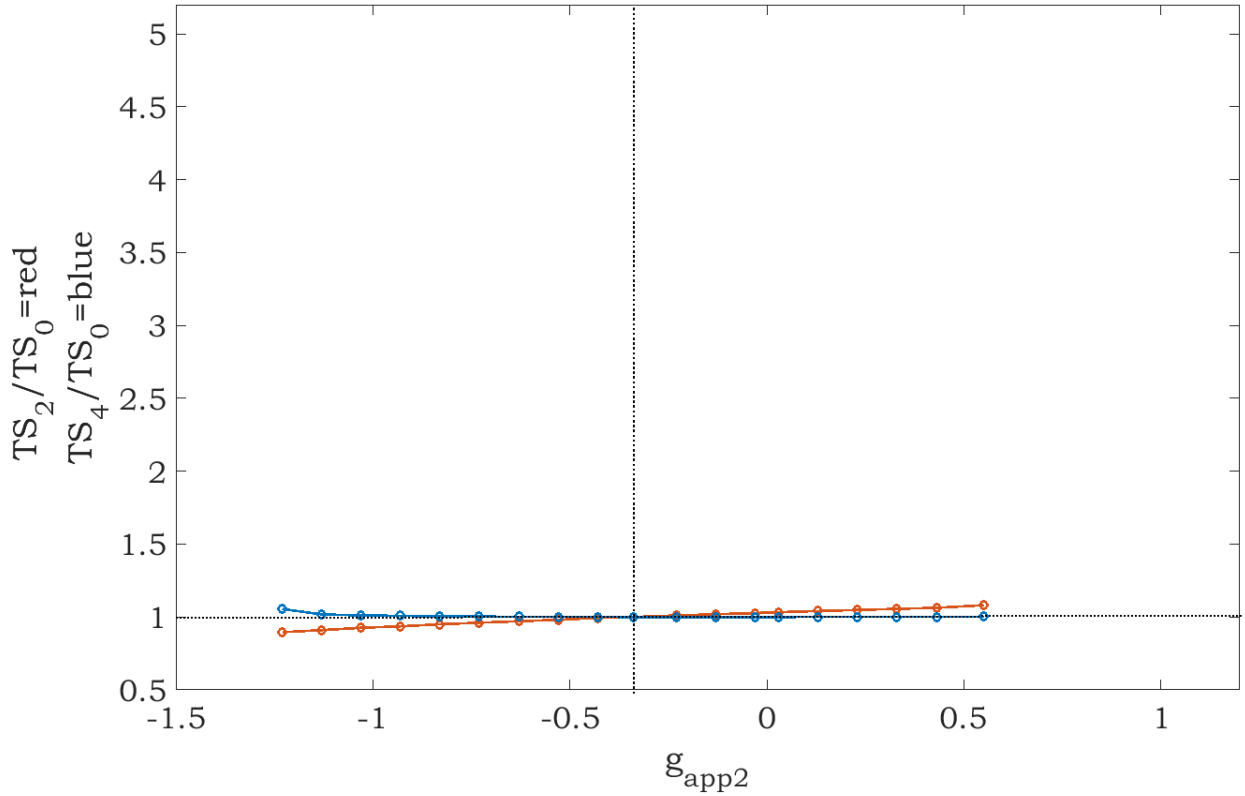

Figure 29: Changes in silent phase duration with changes in g_{app_2}, the drive to cell 2. In each plot, g_{app_4}, was held fixed at g_{app_0}, the baseline drive for the corresponding model (*dotted vertical line*), and g_{app_2} was varied above and below that level. T_{s_2} and T_{s_4} denote the resulting silent phase durations of cells 2 and 4, respectively, and T_{s_0} (*dotted horizontal line*) denotes the silent phase duration with $g_{app_2} = g_{app_4} = \bar{g_{app}}$. Half-center oscillations based on persistent sodium current tuned to inhibitory adapt escape.

5.2 ADAPT EXCITATORY RELEASE MODEL

5.2.1 Half-center oscillation mechanisms

We now know that there is a way to *adapt* the responses by changing the values of the synaptic threshold. In the release mechanism, the synaptic threshold is shifted through the inhibited nullclines for the excitatory cells [30, 33, 8]. Thus, it is now high enough that it is ecountedred by these vells while they are still in their active phase as illustrated in Figure 31. This regime is adjusted to allow the excitatory cells 1 and 3 to drive the transition between the silent and active phases while instigating the same transitions for cells 2 and 4. Yet, once more, we must consider the critical role that the synaptic current may have on the behavior of the neural network.

5.2.1.1 Parameters For the adapt release excitatory regime we list all parameter values necessary to maintain the dynamics, starting with $\alpha = 1$ and:

Excitatory cells	Values	Inhibitory cells	Values
g_{nap_E}	8.0	g_{nap_I}	5.0
g_{l_E}	2.0	g_{l_I}	4.0
g_{syn_E}	1	g_{syn_I}	3
$g_{app_{1,3}}$	0.815	$g_{app_{2,4}}$	-0.19
θ_{m_E}	- 31.0	θ_{m_I}	-34.0
σ_{m_E}	-5.0	σ_{m_I}	-6.0
θ_{h_E}	- 47.0	θ_{h_I}	-34.0
σ_{h_E}	8.0	σ_{h_I}	8.0
θ_{syn_E}	- 10.0	θ_{syn_I}	-30.0
σ_{syn_E}	-4.0	σ_{syn_I}	-4.0

Table 7: We consider the set parameters necessary to maintain a regime of intrinsic escape model with different set values for inhibitory and excitatory cells.

In Figure 31, the trajectories of the solutions seen are almost identical to those seen in both release regimes in **Chapter 4**. However, the main changing feature that allows for this oscillatory response is the synaptic threshold (as indicated by the dotted lines in Figure 31) that is particularly shifted for the "inhibitory cells", while the synaptic threshold of the excitatory cells is still within the trajectory in phase I.

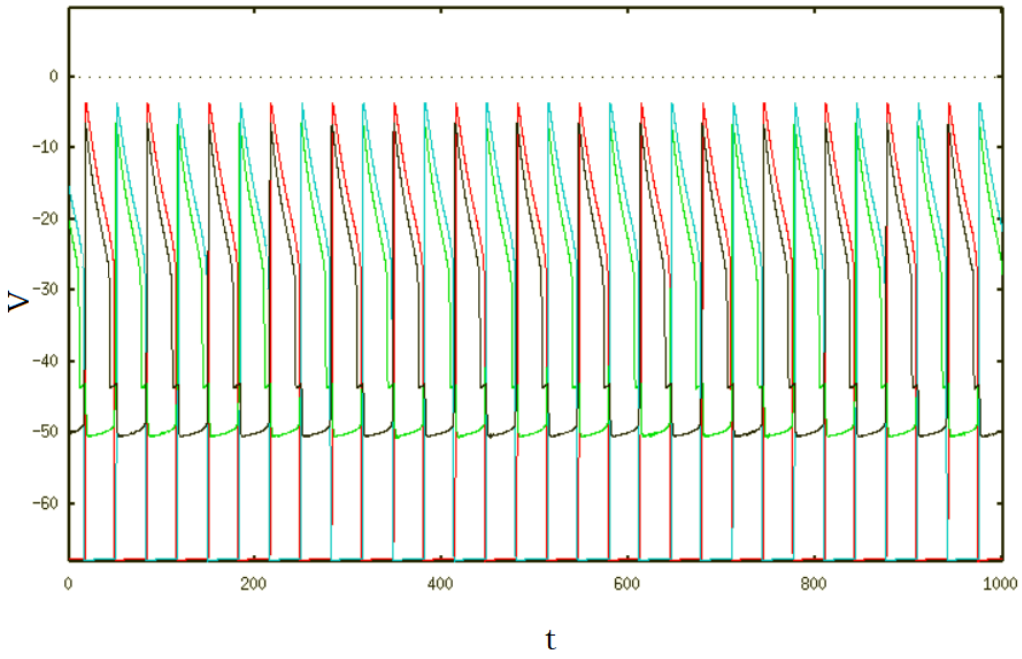

Figure 30: Time courses for periodic oscillations of (cell 1 (black), cell 2 (red), cell 3 (green), cell 4 (blue)) set to an excitatory adapt release regime

We see that the trajectory of cells 1 and 3 follows close to the uninhibited blue v-nullcline in phase I for cell 1 and phase III for cell 3. Moreover, the trajectory of the excitatory cells manage to reach the right knee of the uninhibited nullcline. The position of the synaptic threshold, denoted by the dotted line, for the excitatory cells are prescribed as $\theta_{syn_E} = -10$; see Table 7, such that it does not intersect with the transition phase between silent and active states in cells 1 and 3. On the other hand, the synaptic threshold for cells 2 and 4 is $\theta_{syn_I} = -30$; see Table 7. However, the synaptic input of inhibitory cells have voltage transition values between silent and active phases in both sides of the synaptic threshold.

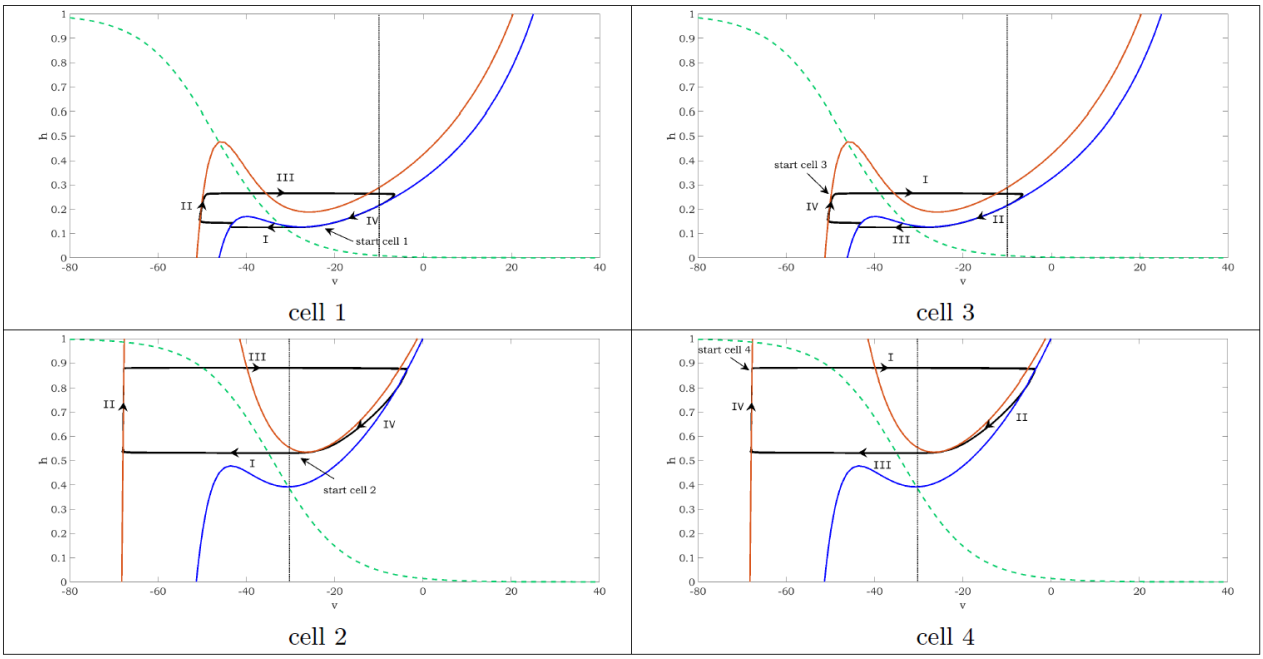

Figure 31: Basic nullcline configurations and periodic orbits for four cell connections with half-center oscillation mechanism tuned to an excitatory adapt release regime. The solid lines are v-nullclines. The red cubic curves represents the inhibited v-nullclines while the blue curves represent the uninhibited v-nullcline for cells 1 and 3. For cells 2 and 4 the red cubic curves represents its unexcited v-nullclines while the blue curves represent their excited v-nullcline. The dashed green line are slow variable nullclines, thick black line are trajectories corresponding to half-center oscillation, and dotted line shows synaptic threshold.

In Figure 31, cell 1 and cell 2 are initially both in the active phase I. Cell 1 is positioned in the blue uninhibited v-nullcline while cell 2 is slightly below the right knee of its unexcited v-nullcline although it is currently governed by the unexcited nullcline. Cell 1 is currently exciting cell 2. And this allows cell 2 to inhibit cell 3, which is at the top end of silent phase IV in the inhibited red nullcline as is cell 4. Thus, Cell 3 is silent and unable to excite cell 4. However, once cell 1 crosses its synaptic threshold, it stops exciting cell 2. As cell 2 crosses its synaptic threshold, cell 3 is *released* from inhibition and is able to transition to the uninhibited nullcline. As this happens, cell 3 begins to excite cell 4 which in return crosses its synaptic threshold and begins to inhibit cell 1. Cell 1 must now transition to the

inhibited nullcline. Due to the fast dynamics, it has a small jump in its trajectory as we see the transitions from the blue unihibited nullcline to the red inhibited one in its phase I. As cell 1 becomes inhibited, cell 2 is no longer excited and thus, also reaches its unexcited nullcline. At this point cells 1 and 3 have switched positions, as have cells 2 and four. This marks half of the oscillation.

5.2.2 Control of oscillation period and phase duration

5.2.2.1 Symmetric case Since this model is tuned to the adapt *excitatory* release regime, we know that the model relies heavily on the drive of the *excitatory* cells to initiate the dynamics of the system. Therefore, we will consider how changing the drive g_{appE} of cells 1 and 3 may influence the periodic solutions of this model now that we have the additional shift in input of the synaptic current.

For the symmetric case, we will consider excitatory cells 1 and 3 to be under the influence of the same applied drive g_{app_E}. We will vary the drive uniformly while maintaining a periodic half-center solution and staying within the dynamics of the regime. The regime maintain solutions at a minimum value for $g_{app_E(min)} = 0.44$ and max value set at $g_{app_E(max)} = 1.09$. These values give us a midpoint $g_{\bar{app}_E} = 0.815$ as seen in Table 7 and we will consider it our *baseline drive*. The nullclines for these applied drive values are illustrated in Figure 33. We see that at $g_{appE(min)}$ will soon lose a fixed point on the left knee of the inhibited purple nullcline. Also, at $g_{app_E(max)}$ we see that we now have a fixed point on the middle branch of the inhibited nullcline while the uninhibited nullcline starts to loose its cubic shape. Thus, the mechanism of the regime changes and the parameters prescribed for this method Table 7 no longer are able to support an oscillatory response out of the range described by at $g_{app_E(max)}$ and at $g_{app_E(min)}$.

The change of g_{app_E} in relation to the range of the total divided by $g_{\bar{app}}$ yields the relative range of the period T, which is normalized with the period $\bar{T}$ obtained form using the baseline $g_{\bar{app}_E}$ drive. We find that $\Delta T/\Delta g_{app_E}$ is the relative change of T compared to the relative range of g_{app_E}, illustrated in Figure 32. Similar to the intrinsic release cases, we find that as we increase the drive g_{app_E} , the period of oscillation responses increase and yields a range

similar to that seen in the intrinsic release regime, as was illustrated in Figure 33.

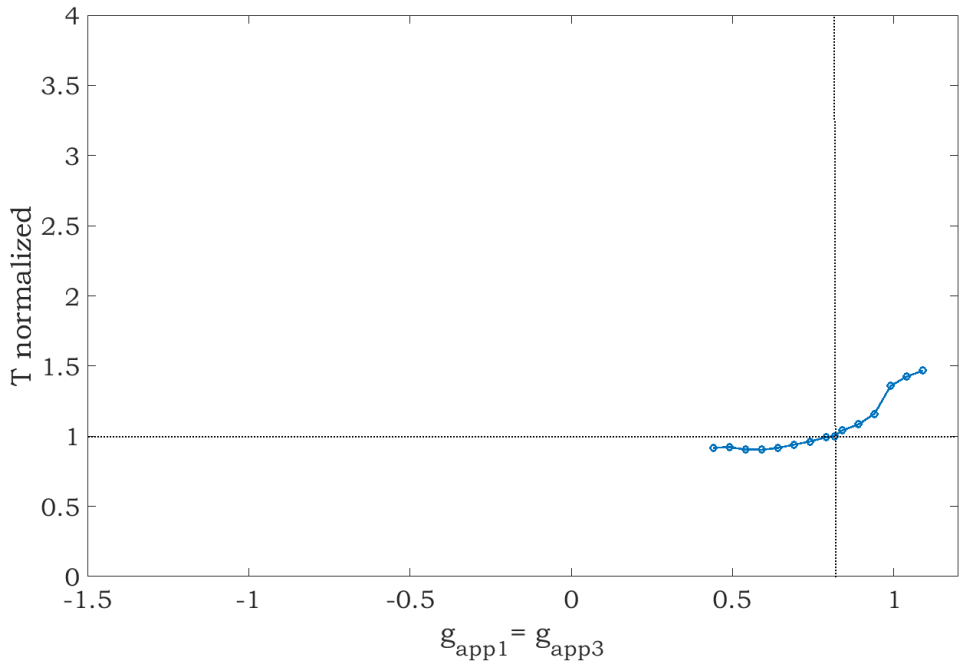

Figure 32: The periods of the basic periodic orbits shown in Figure 30 change with changes in drive to both cells 1 and 3

5.2.2.2 Asymmetric case We are now interested in the response to changes in drive for only one of the excitatory cells. Cell 1 is chosen arbitrarily to receive the additional drive which will correspond to $g_{app_1} \neq g_{app_3}$, other than at its *baseline drive* which g_{app_3} is set to throughout. Notice that the period of g_{app_3} maintains itself nearly constant throughout uniform increases of g_{app_1}. Moreover, the period of cell 1 increases as g_{app_1} increases throughout. Figure 34

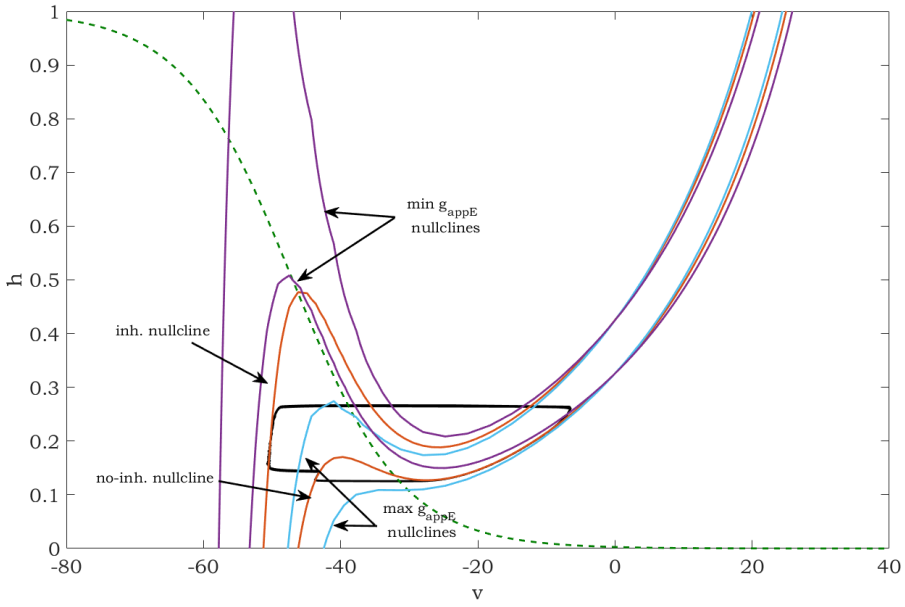

Figure 33: **Nullcline variation changes of g_{appE} of excitatory cells:** The red nullclines represents the inhibited and uninhibited v-nullclines set at its baseline g_{appE} drive. The purple nullclines shows the shift of the v inhibited and uninhibited nullclines at $g_{appE(max)}$.The light blue nullclines shows the shift of the v inhibited and uninhibited nullclines at $g_{appE(min)}$

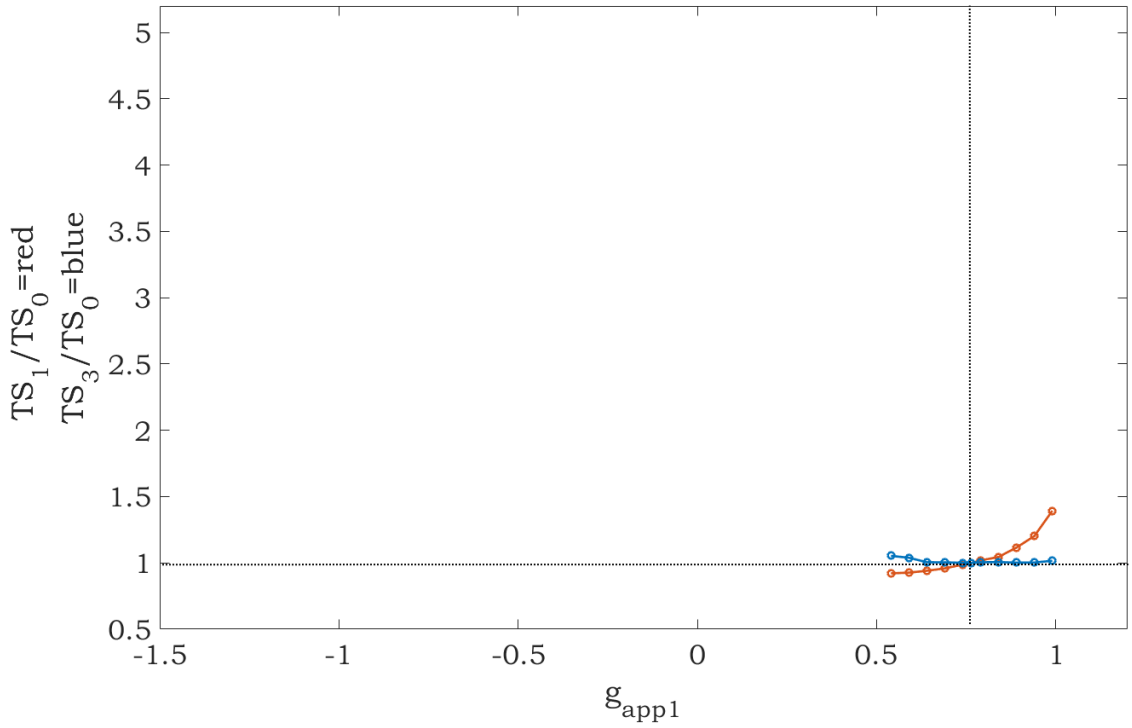

Figure 34: Changes in silent phase duration with changes in g_{app_1}, the drive to cell 1. In each plot, g_{app_3}, was held fixed at g_{app_0}, the baseline drive for the corresponding model (dotted vertical line), and g_{app_1} was varied above and below that level. T_{s_1} and T_{s_3} denote the resulting silent phase durations of cells 1 and 3, respectively, and T_{s_0} denotes the silent phase duration with $g_{app_1} = g_{app_3} = \bar{g_{app}}$. Half-center oscillations based on persistent sodium current tuned to excitatory adapt release.

6.0 CONCLUSIONS

In the introduction, we saw that a wide range of models have been proposed and analyzed the physical interactions of animals with a wide variety of motions and repetitive behaviors (walking, breathing, scratching, and others) that are driven by interacting populations of spiking neurons called CPGs. The complexity of such networks of spiking neurons create a complex mathematical analysis[11, 12, 14, 18, 26].

More simplified models can produce significant responses representing the network in which they are embedded [25]. These have allowed for further investigation and analysis of different configurations of locomotion activity. It has been noted that a single neuron may characterize a population of neurons in which the average voltage is representative of a population set and their output activity. This simplification has allowed for a more general description of the behavior of the populations through its silent and active states[22, 21]. We have constructed a model of a CPG network of coupled half-center oscillators. The architecture of the connections considers a sodium conductance-based modeled for cells that are synaptically coupled to study functional connection patters. However, we aim to create a model that features a more biophysical representation of locomotion activity.

We have studied the capacity for our CPG network model to operate in many different regimes and generate oscillatory responses. Our objective was to compose and investigate the adaptability of CPG oscillatory responses to different modifications of drive and synaptic input. We also focused on investigating how we can adapt network connections with different parameter choices that manage values of the input drives and also the intrinsic properties of the dynamical systems of the CPG models. The architecture of our model can stably reproduce fundamental locomotion responses of phase transition rhythms through alternation of excitatory-inhibitory burst synchronization throughout all the different regimes.

In particular, we aim to understand how the duration of the period of oscillations can be changed through different inputs of external drives to the half-centers of the cells that are in charge of initiating the dynamics within their own regime. The cases of controlled drive studied are of symmetric and asymmetric types, as described in **Chapter 2**. In the symmetric case, we found that based on the regime and functions of each cell within it, either the excitatory or inhibitory cells will be set to a constant input drive. Simultaneously, the drive of the cells in charge of initiating the dynamics are paired and varied throughout. The second case is of asymmetric nature. Once again, based on the regime and functions of each cell within it, either the excitatory or inhibitory cells will be set to a constant drive as well as one of the driving cells while varying ***one*** cells drive through a range of inputs.

Our mathematical analysis provides insight into the specific factors that contribute to the phase plane dynamics of each model and into different responses gathered through tuning of input drives. The difference in responses yields a better understanding of how the variation of drive inputs contribute to the responses of the oscillatory solutions. We use a generalization of the mathematical analysis in all the regimes studied while using the same model structure throughout. Thus, significant variations of parameters helped achieve the different regimes of escape and release mechanisms described in **Chapters 3-5**. The generalizations that have been considered, are useful in providing further insight into the effects that drive modulation may have on the responses while comparing the results obtained through the different regimes.

Each model's regimes have illustrated the changes in active phase duration through a range of values of $g_{app(I,E)}$. First, we analyzed the oscillatory responses within the symmetric case. In particular, we quantify the ranges of solutions found in all analyzed cases as seen in Table 8. This table presents the relative range of $g_{app(I,E)}$ that was varied, which is case dependent, over the oscillatory solutions in which the regime was maintained. Therefore, we are able to obtain Δg_{app} which is defined as $g_{app(I,E)}$ over its baseline drive g_{app0} and is observed in the asymmetric case.

In Table 9, we also find a quantitative result that summarizes the different changes in active phase durations for inhibitory cells and excitatory cells pertinent to the regime in which they are functioning. These responses were illustrated within all regimes of asymmetric

case analysis. Additionally, T_{Sj} is defined as the relative range of active phase durations for either the excitatory or inhibitory cells cells depending on which ones are driving the phase transitions. These were then divided by the period at the baseline drive $\bar{T}$ in order to normalize our results. Lastly, we define the ratio between ranges of T_{Sj} and oscillation periods as $\Delta T_{Sj}/\bar{T}$, for either excitatory or inhibitory cells, representing a measure of phase independence or the degree of changes in period. These are due to changes in $g_{app(I,E)}$ that modify the solution for the active phase duration.

Model Regime	$\hat{g_{app}}$	g_{app} **range**	Δg_{app}	T **range**	$\Delta T/\Delta g_{app}$
Excitatory Escape	0.275	0.15	0.546	2.987	5.47
Excitatory Release	0.36	0.58	1.611	0.57	0.35
Excitatory Adapt Release	0.815	0.65	0.798	0.549	0.687
Inhibitory Escape	0.185	0.23	1.243	2.15	1.73
Inhibitory Release	-0.05	0.32	6.4	0.424	0.066
Inhibitory Adapt Escape	0.495	1.78	3.6	0.185	0.05

Table 8: Changes in period oscillations and drive conductances in the symmetric case.

Table 8 and Table 9 provide results that oscillations produced in all models. The results in Table 8 shows that excitatory cells provide overall a larger range of period activity with respect to the changes to the g_{app} throughout all methods of escape and release. Therefore, it is valid to say that systems should consider the excitatory cells as the more flexible and independent within their network.

In Table 9 we clearly we see that the inhibitory release and inhibitory adapt escape models show very high stability with half-center oscillations that exist over a wide range of values of the g_{appI} drives in both symmetric and asymmetric cases. However, they both show a significant insensitivity of the period to g_{appI}. Interestingly, both models are of the inhibitory regimes where the inhibitory cells are the ones responsible for initiating the dynamics of the system. Also, the excitatory intrinsic release and inhibitory intrinsic escape models also show high stability with half-center oscillations over a wide range of values of

Model Regime	$\hat{g_{app}}$	g_{app1} **range**	Δg_{app}	T_{S_1} **range**	T_{S_3} **range**	$\Delta T_{S_1}/\Delta T$	$\Delta T_{S_3}/\Delta T$
E-Escape	0.275	0.15	0.545	0.027	3.03	0.009	1.009
E-Release	0.36	0.56	1.56	0.518	0.053	1.114	0.114
E-Adapt Release	0.815	0.52	0.64	0.543	—-0.0005—	1.001	0.001
Model Regime	$\hat{g_{app}}$	g_{app2} **range**	Δg_{app}	T_{S_2} **range**	T_{S_4} **range**	$\Delta T_{S_2}/\Delta T$	$\Delta T_{S_4}/\Delta T$
I-Escape	0.185	0.248	1.34	0.01466	4.23	0.003	1.0035
I-Release	-0.05	0.31	6.2	0.419	0.056	1.154	0.154
I-Adapt Escape	0.495	1.78	3.6	0.185	0.053	1.402	0.402

Table 9: Changes in the drive conductances and active phase durations.

g_{app} drives, yet significantly smaller than the previously mentioned cases. Moreover, we see that the intrinsic excitatory and release regimes as well as the adapt escape regimes show the greatest range of phase duration in the symmetric case and independence in phase duration control as seen in the symmetric case.

While many of these results are similar to those presented in Daun [8] it is important to note certain pertinent differences when comparing their results to our four cell model. They found that the postinhibitory rebound model (release model) and one of the calcium adaptation cases showed high stability over a large range of drive g_{app} where both of their cells received the same drive and in cases of drive asymmetry. Also, they found that they had the least ability of independence to change phase durations via asymmetric drive. However, they also noticed that it is their persistent sodium current based model that showed the greatest independence to change phase durations via asymmetric drive which is similar to our findings, however as previously mentioned the excitatory adapt release regime showed the greates independence to change phase durations overall.

Never-the-less, their results are similar to ours when analyzing the great sensitivity in the periodic response through changes of g_{app} drive and exhibiting the largest range of periods.

Model Regime	$\hat{g_{app}}$	g_{app1} **range**	T_{S_1} **range**	T_{S_2} **range**	$\Delta T_{S_1}/\Delta T$	$\Delta T_{S_2}/\Delta T$
Persistent sodium	0.235	0.438	2.30	0.0167	0.993	0.007
Postinhibitory rebound	0.05	2.4	0.0582	0.181	0.243	1.47
Adaptation, case 1	0.815	0.270	0.544	-0.0187	1.04	0.036
Adaptation, case 2	0.63	1.43	0.722	-1.49	0.624	1.94

Table 10: Table 2 in Daun et al. [8] paper of changes in drive conductances and silent phase durations in the asymmetric case. However, last column was added for purposes of comparing to our models

Thus, we see that considering which active cell initiates the dynamics and the mechanism of the regimes play key roles in the oscillatory responses and phase transitions of the network. The limitations of the biological CPG network proposed is unknown. Further, understanding of different forms of normal locomotion activity is necessary to understand the cross-cord and lateral coupling symmetry of the system.

Similar networks have been widely studied in both *in vitro* and *in vivo* experiments of midbrain simulations. They found that left and right coordination may overlap during different gates and extensor flexor ipsilateral connections could potentially maintain different periods through locomotion without varying the gate in which they are responding. Also, they found that asymmetric activation of flexors and extensors may provide insight into the locomotion of animals that are able to maintain normal gaits.[14, 32, 35],

Although oscillations in most CPGs is still a mystery, it is very useful to know that CPGs can be very flexible and are able to adapt to oscillatory patterns that their networks generate. As previous studies have discovered, we have witnessed that the flexibility of CPGs helps with the ability the model has generated oscillations through a large range of frequencies while under the influence of descending drives; see [8, 23]. Due to the fact that we aim to provide some biological context to our CPG network, we find that a half-center model is very

helpful studying how the dynamics of the mechanism can provide us with more flexibility.

Our main focus was on the reduced models proposed by Daun et al. [8] while adding another level of complexity to the architecture of the network and considering the dynamics represented through phase plane analysis. It is to be expected that more complex networks that feature phase transitions through different mechanisms are yet to be further analyzed. Future research should focus on understanding some of the results presented throughout this study which may be present in different biologically relevant CPG networks.

BIBLIOGRAPHY

[1] *Front Matter*. pp. i–xiv.

[2] Brown, T. G. Mechanisms of oscillation in dynamic clamp constructed two-cell half-center circuits. *Royal Society 84*, 572 (12 1911), 308–319.

[3] Brown, T. G. On the nature of the fundamental activity of the nervous centres; together with an analysis of the conditioning of rhythmic activity in progression, and a theory of the evolution of function in the nervous system. *Journal of Physiology 48*, 1 (3 1914), 18–46.

[4] Butt, S. J., Lebret, J. M., and Kiehn, O. Organization of leftright coordination in the mammalian locomotor network. *Brain Research Reviews 40*, 1 (2002), 107 – 117.

[5] Butt, S. J. B., and Kiehn, O. Functional identification of interneurons responsible for left-right coordination of hindlimbs in mammals. *Neuron 64*, 38 (6 2003), 953–963.

[6] Calabrese, R. L., and Schutter, E. D. Motor-pattern-generating networks in invertebrates: modeling our way toward understanding. *Trends in Neurosciences 15*, 11 (1992), 439 – 445.

[7] C.PerretJ, M.Cabelguen, and D.OrsalC. Analysis of the pattern of activity in knee flexor motoneurons during locomotion in the cat. *Stance and Motion* (1988), 133–141.

[8] Daun, S., Jonathan E, . R., and Rybak, I. A. Mechanisms of left-right coordination in mammalian locomotor pattern generation circuits: A mathematical modeling view. *Journal of Computational Neuroscience 27*, 1 (1 2009), 1–36.

[9] Hill, A., Hooser, S., and L Calabrese, R. Half-center oscillators underlying rhythmic movements, 01 2002.

[10] Ivashko, D., Prilutsky, B., Marking, S., CHapin, J., and Rybak, I. *Neurocomputing*.

[11] Jankowska, E., Jukes, M. G. M., Lund, S., and Lundberg, A. The effect of dopa on the spinal cord 5. reciprocal organization of pathways transmitting excitatory

action to alpha motoneurones of flexors and extensors. *Acta Physiologica Scandinavica 70*, 3-4 (1967), 369–388.

[12] Jankowska, E., Jukes, M. G. M., Lund, S., and Lundberg, A. The effect of dopa on the spinal cord 6. half-centre organization of interneurones transmitting effects from the flexor reflex afferents. *Acta Physiologica Scandinavica 70*, 3-4 (1967), 389–402.

[13] Kiehn, O. Development and functional organization of spinal locomotor circuits. *Current Opinion in Neurobiology 21*, 1 (2 2011), 100–109.

[14] Kiehn, O., Kjaerulff, O., Tresch, M. C., and Harris-Warrick, R. M. Contributions of intrinsic motor neuron properties to the production of rhythmic motor output in the mammalian spinal cord. *Brain Research Bulletin 53*, 5 (2000), 649 – 659.

[15] Kjaerulff, O., and Kiehn, O. Distribution of networks generating and coordinating locomotor activity in the neonatal rat spinal cord in vitro : A lesion study. *Journal of Neuroscience 16*, 18 (1996), 5777–5794.

[16] Marder, E., and Calabrese, R. L. Principles of rhythmic motor pattern generation. 687–717.

[17] McCrea, D. A., and Rybak, I. A. *Brain Research Reviews*.

[18] Molkov, Y. I., Bacak, B. J., Talpalar, A. E., and Rybak, I. A. Mechanisms of left-right coordination in mammalian locomotor pattern generation circuits: A mathematical modeling view. *Computational Biology 97*, 1 (3 2015), 1–40.

[19] Nishimaru, H., Restrepo, C. E., and Kiehn, O. Activity of renshaw cells during locomotor-like rhythmic activity in the isolated spinal cord of neonatal mice. *Journal of Neuroscience 26*, 20 (2006), 5320–5328.

[20] Rabe, N., Gezelius, H., Vallstedt, A., Memic, F., and Kullander, K. Netrin-1-dependent spinal interneuron subtypes are required for the formation of left-right alternating locomotor circuitry. *Journal of Neuroscience 29*, 50 (2009), 15642–15649.

[21] Rubin, J. E., Bacak, B. J., Molkov, Y. I., Shevtsova, N. A., Smity, J. C., and Rybak, I. A. Interacting oscillations in neural control of breathing: modeling and qualitative analysis. *Journal of Computational Neuorscience 30*, 3 (6 2011), 607–632.

[22] Rubin, J. E., Shevtsova, N. A., Ermentrout, G. B., Smith, J. C., and Rybak, I. A. Multiple rhythmic states in a model of the respiratory central pattern generator. *Journal of Neurophysiology 101*, 4 (4 2009), 2146–2165.

[23] Rybak, I. A., Shevstova, N. A., and Kiehn, O. *The Journal of Physiology*.

[24] Schwemmer, M. A., and Lewis, T. J. Bistability in a leaky integrate-and-fire neuron with a passive dendrite. *SIAM Journal on Applied Dynamical Systems 11*, 1 (2012), 507–539.

[25] Sharp, A. A., Skinner, F. K., and Marder, E. *The American Physiological Society*.

[26] Sherwood, W. E., Harris-Warrick, R., and Guckenheimer, J. *Journal of Computational Neuroscience*.

[27] Shevtsova, N. A., Talpalar, A. E., Markin, S. N., Harris-Warrick, R. M., Kiehn, O., and Rybak, I. A. *The Journal of Physiology*.

[28] Shevtsova, V., Gaponenko, Y., Sechenyh, V., Melnikov, D., Lyubimova, T., and Mialdun, A. Dynamics of a binary mixture subjected to a temperature gradient and oscillatory forcing. *Journal of Fluid Mechanics 767* (2015), 290322.

[29] Shevtsova, V., Gaponenko, Y., Sechenyh, V., Melnikov, D., Lyubimova, T., and Mialdun, A. Dynamics of a binary mixture subjected to a temperature gradient and oscillatory forcing. *Journal of Fluid Mechanics 767* (2015), 290322.

[30] Skinner, F. K., Kopell, N., and Marder, E. Mechanisms for oscillation and frequency control in reciprocally inhibitory model neural networks. *Journal of Computational Neuroscience 1*, 1 (3 1994), 69–87.

[31] Stein, P., Victor, J., Field, E., and Currie, S. Bilateral control of hindlimb scratching in the spinal turtle: contralateral spinal circuitry contributes to the normal ipsilateral motor pattern of fictive rostral scratching. *The Journal of Neuroscience 15*, 6 (1995), 4343–4355.

[32] Talpalar, A. E., Endo, T., Löw, P., Borgius, L., Martin Hägglund, K. J. D., Ryge, J., Hnasko, T. S., and Kiehn, O. Identification of minimal neuronal networks involved in flexor-extensor alternation in the mammalian spinal cord. *Neuron 71*, 6 (9 2011), 1071–1084.

[33] Wang, X.-J., and Rinzel, J. Alternating and synchronous rhythms in reciprocally inhibitory model neurons. *Neural Computation 4*, 1 (1 1992), 84–97.

[34] Weaver, A. L., Roffman, R. C., J.Norris, B., and Calabrese, R. L. A role for compromise: Synaptic inhibition and electrical coupling interact to control phasing in the leech heartbeat cpg. *Frontiers in Behavioral Neuroscience 38* (2010).

[35] Yakovenko, S., McCrea, D. A., Stecina, K., and Prochazka., A. *Journal of Neurophysiology*.

[36] Zhang, C., and Lewis, T. J. Phase response properties of half-center oscillators. *Journal of Computational Neuroscience 35*, 1 (8 2014), 55–74.

[37] Zhong, G., Shevtsova, N. A., Rybak, I. A., and Harris-Warrick, R. M. Neuronal activity in the isolated mouse spinal cord during spontaneous deletions in fictive locomotion: insights into locomotor central pattern generator organization. *The Journal of Physiology 590*, 19 (2012), 4735–4759.